Stockholm University

In Light of Ionic Materials

A short exploration of ionic materials for light-related applications

Brando Adranno

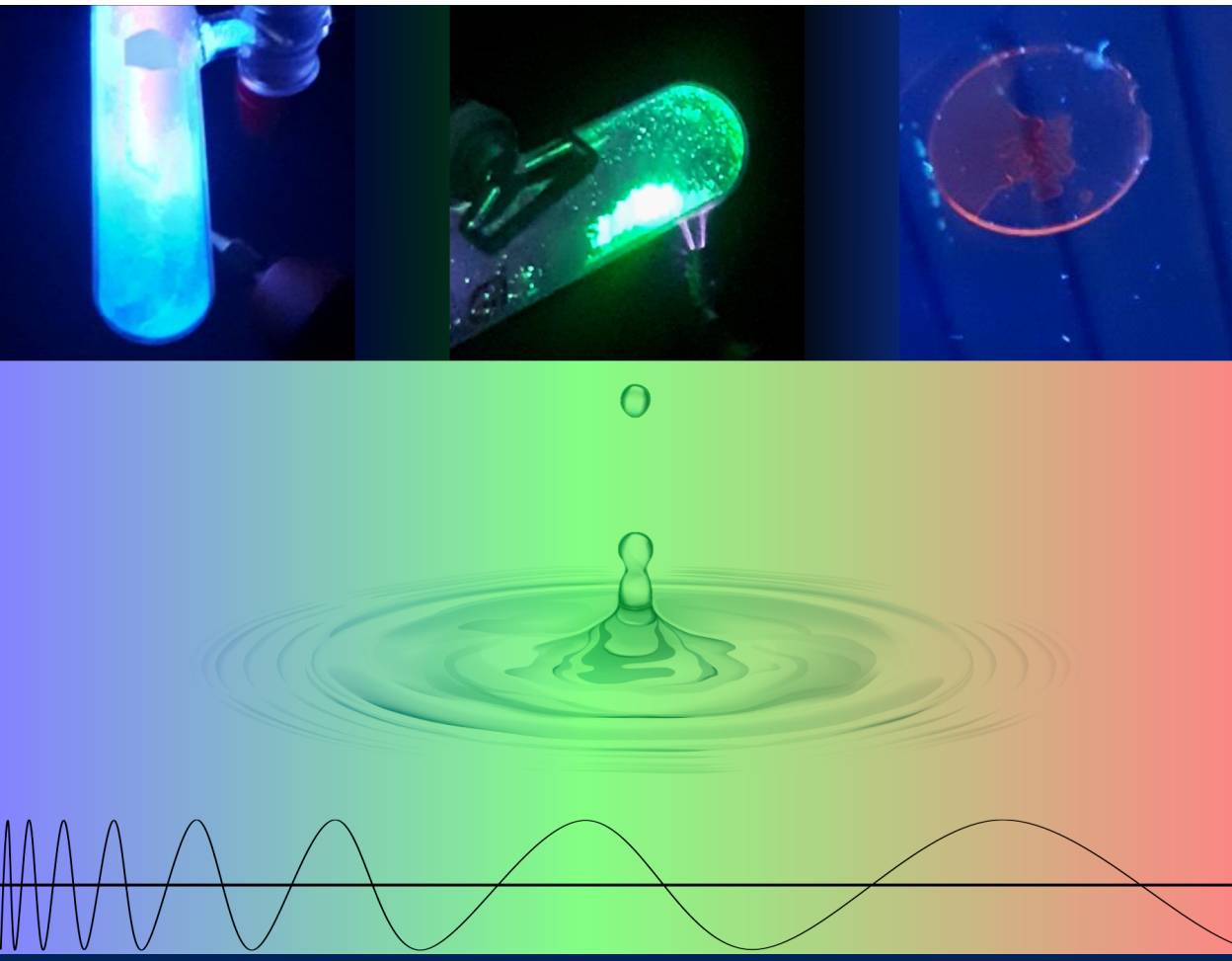

Doctoral Thesis in Materials Chemistry at Stockholm University, Sweden 2022

In Light of Ionic Materials

A short exploration of ionic materials for light-related applications

Brando Adranno

Academic dissertation for the Degree of Doctor of Philosophy in Materials Chemistry at Stockholm University to be publicly defended on Thursday 15 December 2022 at 13.00 in Nordenskiöldsalen, Geovetenskapens hus, Svante Arrhenius väg 12 and online via Zoom, public link is available at the department website.

Abstract

Ionic liquids (ILs) have been one of the most attractive classes of materials of the last decades. The reason behind this is their peculiar set of properties, which enable their possible application in several research fields. ILs are salts that exhibit a very low melting point, which has been arbitrarily defined to be below 100 °C. Due to their ionic nature, ILs have little to no vapor pressure and they often demonstrate good electrical conductivity and high thermal and electrochemical stability. In this work, the focus is directed toward the exploitation of ILs for the engineering of materials that can have a primary role in light-emitting or light-absorbing devices. Materials belonging to the first type are explored in Papers I-III, while the ones belonging to the second are tackled in Papers IV and V.

There has always been a struggle to find a balance between costs and the efficiency of emitting materials for application in dedicated devices. In Papers I-III, two strategies are taken into account to address this issue. Finding inspiration from ionic complexes of Mn(II), newly designed ionic materials and ILs emitting green light are proposed as an alternative to the more expensive heavy metals-based ones such as Ir(III) and Pt(II). Coming closer to an ideal compromise of cost and performance, fully organic and extremely cheap low-melting salts based on the 8-hydroxyquinoline unit were prepared. These compounds revealed efficient fluorescence in the blue region of the spectrum for such simple molecules, paving the way for the preparation of possibly inexpensive light-emitting devices.

In Paper IV, direct absorption of light is taken into consideration with photoresponsive ionic liquids, which undergo *cis-trans* isomerization. Due to this feature and their ionic nature, these materials could be adopted into photoswitches. Additionally, the effect of functional groups on the isomerization of the ILs and on the ability of the materials to undergo mesophase formation was studied.

One of the key components of dye-sensitized solar cells is the electrolytic mediator sandwiched between two electrodes. This has been a matter of intense study due to issues regarding its stability, which impair the device's performance. ILs can be adopted in devices to solve this issue. In Paper V, triazolium ILs allowed the manufacturing of devices with higher efficiencies and longer lifetimes than the ones realized with imidazolium relatives. These materials allowed for the stability of the ionic couple I^-/I_3^- and moisture resistance due to their non-hygroscopic nature.

Keywords: *ionic materials, ionic liquids, mesophases, light-emission, electrochemical applications.*

Stockholm 2022
http://urn.kb.se/resolve?urn=urn:nbn:se:su:diva-210110

ISBN 978-91-8014-040-9
ISBN 978-91-8014-041-6

Department of Materials and Environmental Chemistry (MMK)

Stockholm University, 106 91 Stockholm

Stockholm University

IN LIGHT OF IONIC MATERIALS

Brando Adranno

Stockholm University

In Light of Ionic Materials

A short exploration of ionic materials for light-related applications

Brando Adranno

ISBN print 978-91-8014-040-9
ISBN PDF 978-91-8014-041-6

Printed in Sweden by Universitetsservice US-AB, Stockholm 2022

To my Family and
Friends.

Abstract

Ionic liquids (ILs) have been one of the most attractive classes of materials of the last decades. The reason behind this is their peculiar set of properties, which enable their possible application in several research fields. ILs are salts that exhibit a very low melting point, which has been arbitrarily defined to be below 100 °C. Due to their ionic nature, ILs have little to no vapor pressure and they often demonstrate good electrical conductivity and high thermal and electrochemical stability. In this work, the focus is directed toward the exploitation of ILs for the engineering of materials that can have a primary role in light-emitting or light-absorbing devices. Materials belonging to the first type are explored in Papers I-III, while the ones belonging to the second are tackled in Papers IV and V.

There has always been a struggle to find a balance between costs and the efficiency of emitting materials for application in dedicated devices. In Papers I-III, two strategies are taken into account to address this issue. Finding inspiration from ionic complexes of Mn(II), newly designed ionic materials and ILs emitting green light are proposed as an alternative to the more expensive heavy metals-based ones such as Ir(III) and Pt(II). Coming closer to an ideal compromise of cost and performance, fully organic and extremely cheap low-melting salts based on the 8-hydroxyquinoline unit were prepared. These compounds revealed efficient fluorescence in the blue region of the spectrum for such simple molecules, paving the way for the preparation of possibly inexpensive light-emitting devices.

In Paper IV, direct absorption of light is taken into consideration with photoresponsive ionic liquids, which undergo *cis-trans* isomerization. Due to this feature and their ionic nature, these materials could be adopted into photoswitches. Additionally, the effect of functional groups on the isomerization of the ILs and on the ability of the materials to undergo mesophase formation was studied.

One of the key components of dye-sensitized solar cells is the electrolytic mediator sandwiched between two electrodes. This has been a matter of intense study due to issues regarding its stability, which impair the device's per-

formance. ILs can be adopted in devices to solve this issue. In Paper V, triazolium ILs allowed the manufacturing of devices with higher efficiencies and longer lifetimes than the ones realized with imidazolium relatives. These materials allowed for the stability of the ionic couple I^-/I_3^- and moisture resistance due to their non-hygroscopic nature.

Sammanfattning

Jonvätskor (JV) har uppstått som en attraktiv klass av material under de senaste decennierna. Anledningen till detta är deras unika egenskaper, vilka har möjliggjort tillämpningar inom flera olika forskningsområden. JV är salter som har en mycket låg smältpunkt, där den övre gränsen godtyckligt definierats vid 100 °C. I och med deras joniska natur så har JV ett lågt eller obefintligt ångtryck och de uppvisar ofta god elektrisk och termisk konduktivitet samt hög elektrokemisk stabilitet. Forskningen som utgör denna avhandling har fokuserat på att nyttja JV för att skapa material som kan ha en primär roll i ljusemitterande och ljusabsorberande enheter. Material som lämpar sig för det förstnämnda användningsområdet, ljusemission, har utforskats i de tre första artiklarna (Paper I-III). I de två sista artiklarna (Paper IV and V) har material för ljusabsorption studerats.

Balansen mellan kostnad och effektivitet är en ständig avvägning i utvecklandet av ljusemitterande enheter. I den första gruppen av artiklar har två strategier använts för att hjälpa med detta. Genom att ta inspiration från jonkomplex av Mn(II) så har nya joniska material och JV som emitterar grönt ljus utvecklats. Dessa föreslås som alternativ till dyrare material gjorda av tungmetaller såsom Ir(III) och Pt(II). I en än mer förfinad avvägning av kostnad och effektivitet så har fullständigt organiska och kostnadseffektiva salter av 8-hydroxikinolin med låg smältpunkt förberetts. Dessa föreningar uppvisar effektiv fluorescens i den blå regionen av ljusspektrumet och banar därmed väg för förberedandet av kostnadseffektiva ljusemitterande material.

I den näst sista artikeln (Paper IV) så har JV använts för den direkta absorptionen av ljus. I detta fall används JV som genomgår en *cis-trans*-isomerisering. Denna effekt, tillsammans med deras joniska natur, gör att de kan användas som ljus-responsiva material. Utöver detta studerades även effekten som olika funktionella grupper har för isomeriseringen, samt huruvida materialen kan bilda olika typer av meso-faser.

En av nyckelkomponenterna i färgsensibiliserade solceller (Grätzelceller) är elektrolytskiktet som finns mellan de två elektroderna. Dess roll har studerats intensivt då låg stabilitet hos elektrolyten är ett vanligt förekommande problem som påverkar solcellens prestanda negativt. JV kan implementeras i solceller för att lösa detta problem. I den sista artikeln (Paper V) så har JV baserade på triazoliumjoner gett solceller med högre effektivitet och en längre livstid än andra JV baserade på imidazoliumjoner. Användandet

av dessa material leder till en stabilisering av jonparet I^-/I_3^- samt ett motstånd mot fukt hos materialen i och med deras icke-hygroskopiska natur.

List of Publications

This thesis is based on the following publications:

I. Complex phase behaviour of organic-inorganic green-emitting ionic manganese halides

Brando Adranno, Veronica Paterlini, Volodymyr Smetana, Guillaume Bousrez, Alexander Ovchinnikov, and Anja-Verena Mudring. Manuscript submitted (2022).

I synthesized the presented material, performed or participated in the majority of the experiments, participated in all data interpretation, and wrote the major part of the draft.

II. Broadband white light-emitting light emitting electrochemical cells

Brando Adranno, Shi Tang, Veronica Paterlini, Volodymyr Smetana, Olivier Renier, Guillaume Bousrez, Ludvig Edman, and Anja-Verena Mudring. Manuscript submitted (2022).

I synthesized the presented material, performed or participated in the majority of the experiments, participated in all data interpretation, and wrote the major part of the draft.

III. The 8-Hydroxyquinolinium Cation as a Lead Structure for Ionic Small Molecules Sky Blue Emitter Materials

Brando Adranno, Olivier Renier, Guillaume Bousrez, Veronica Paterlini, Glib V. Baryshnikov, Volodymyr Smetana, Hans Ågren, Andreas Metlen, Anja-Verena Mudring, and Robin D. Rogers. Manuscript submitted (2022).

I synthesized the presented material, performed or participated in the majority of the experiments, participated in all data interpretation, and wrote the major part of the draft.

IV. Photoisomerization and Mesophase Formation in Azo-Ionic Liquids

Olivier Renier, Guillaume Bousrez, Kathrin Stappert, Magdalena Wilk-Kozubek, Brando Adranno, Hanwen Pei, Eike T. Spielberg, Volodymyr Smetana, and Anja-Verena Mudring
Cryst. Growth Des. **2020,** 20 (1), 214-225

I performed all the synthetic steps for the 1-dodecyl-3-(2-(4-((4-nitrophenyl)diazenyl)phenoxy)ethyl)-imidazolium bromide (**5**) and performed the relative IR and NMR characterization, and determination of the thermal properties. Additionally, I participated in the writing of the manuscript.

V. Ionic Liquid-Based Dye-Sensitized Solar Cells—Insights into Electrolyte and Redox Mediator Design

Guillaume Bousrez, Olivier Renier, Brando Adranno, Volodymyr Smetana, and Anja-Verena Mudring
ACS Sust. Chem. Eng. **2021**, 9, 8107-8114

I performed all the synthetic steps for the 1-hexyl-3-methyl-1,2,3-triazolium iodide (**5**) and the 1-butyl-3-methyl-1,2,3-triazolium iodide (**6**) and performed the relative IR and NMR characterization, and determination of the thermal properties. Additionally, I performed and analyzed the cyclic voltammetry of all the presented materials and participated in the writing of the manuscript.

Paper not included:

Ready Access to Anhydrous Anionic Lanthanide Acetates by Using Imidazolium Acetate Ionic Liquids as the Reaction Medium

Guillaume Bousrez, Olivier Renier, Steven P. Kelley, Brando Adranno, Elnaz Tahavori, Hatem M. Titi, Volodymyr Smetana, Si-Fu Tang, Anja-Verena Mudring, Robin D. Rogers
Chem. Eur. J.. **2021**, *27*, 13181.

Contents

Abbreviations

ACN	Acetonitrile
CE	Counter Electrode
CIE	Commission Internationale de l'Eclairage
C_n	Alkyl chain of *n* C atoms
CV	Cyclic Voltammetry
DSC	Differential Scanning Calorimetry
DSSC	Dye-Sensitized Solar Cell
eq.	Equivalent
EtOAc	Ethyl Acetate
EQE	External Quantum Efficiency
HOMO	Highest Occupied Molecular Orbital
H_2SO_4	Sulfuric Acid
FTO	Fluorine-doped Tin Oxide
HOIP	Organic-Inorganic Hybrid Perovskite
IL	Ionic Liquid
ILC	Ionic Liquid Crystal
im	Imidazolium
LC	Liquid Crystal/Liquid Crystalline
λ_{em}	Emission Wavelength
λ_{ex}	Excitation Wavelength
LUMO	Lowest Unoccupied Molecular Orbital
mim	Methyl-imidazolium
MS	Mass Spectrometry
NMR	Nuclear Magnetic Resonance
PEDOT:PSS	Poly(3,4-ethylenedioxythiophene): Polystyrene Sulfonate
PLQY	Photoluminescence Quantum Yield
P_{nnn} or P_{nnnn}	P atom connected with three or four alkyl chains of *n* C atoms
POM	Polarized Optical Microscopy
ppm	Parts per million
PXRD	Powder X-Ray Diffraction
QY	Quantum Yield
RE	Reference Electrode
RTIL	Room Temperature Ionic Liquid
SCXRD	Single Crystal X-Ray Diffraction

SM	Small Molecule
SmA	Smectic A
SmC	Smectic C
STE	Self-trapped Exciton
TDFT	Time-Dependent Density Functional Theory
Tf_2N	Bis(trifluoromethanesulfonyl)imide
TG	Thermogravimetry
THF	Tetra-Hydro-Furan
WE	Working Electrode

1. Introduction

In this chapter, I will discuss the concepts that are at the base of my work, and they are divided into two sections. In the first one, I will explain the nature of ionic liquids (ILs) and their properties, while in the second one I will discuss light-related phenomena, materials, and devices that will be fundamental for understanding the presented results.

1.1 Ionic liquids (ILs) and their properties

1.1.1 What are ILs?

The story of ionic liquids (ILs) started over a century ago, in 1888, when Gabriel and Weiner reported the low-melting (50 °C) ethanolammonium nitrate.[1] It took more than twenty-five years to observe other examples of salts with similar thermal properties thanks to the work of Walden in 1914 on alkylammonium nitrates.[2] Besides these early discoveries, this class of materials has been thoroughly investigated only in the past decades.

ILs, or low-melting salts, are primarily defined by having a melting point below 100 °C. This is not the only property that made the ILs so attractive to the scientific community. They revealed negligible vapor pressure, non-flammability, medium-to-low viscosity, recyclability, ion conductivity, and high thermal and electrochemical stability.[3,4] Thus, not surprisingly, these properties made them extremely interesting for "green" solvent applications, as an alternative to most common organic solvents.[5,6] Additionally, the high tunability of both their cations and anions, allowed this class of material to be also explored in several different areas.[7–11]

In fact, the nature of the ions can vary a lot, and some examples will be now provided. The most common cations are based on N or P-containing organic molecules such as ammonium, imidazolium, triazolium, tetrazolium, pyridinium, pyrrolidinium, and phosphonium. On the other hand, the type of

anions can space from halides and halogen-containing molecules (such as $[PF_6]^-$, $[BF_4]^-$), to weak organic bases (*i.e.* acetate, alkyl phosphates, and sulfates), to metal complexes. According to the desired application, in the latter case, the metal of choice can be any transition metal, lanthanides, or actinides, while the ligands can be both halogens (most common) or organic-based.[12,13] Some of the ions constituting ILs are collected in **Figure 1**.

The design of the ions involved is the fundamental key to the properties of ILs. Their shape and symmetry have a major role in defining the thermal properties of the final ionic compounds[14] and the ability to form liquid crystalline (LC) phases,[15] which will be discussed more in detail in the following subchapter. The intrinsic mobility and flexibility of the ions involved also have an important role in the properties of the final IL,[16] since these could hinder the crystallization of the material. Finally, specific shapes and functional groups can also affect the properties of the final IL on the basis of the interactions that can be established between the anions and the cations, such as ionic forces, hydrophobic interaction, *van der Waals* forces, hydrogen bonds, π-stacking, and so on.[17]

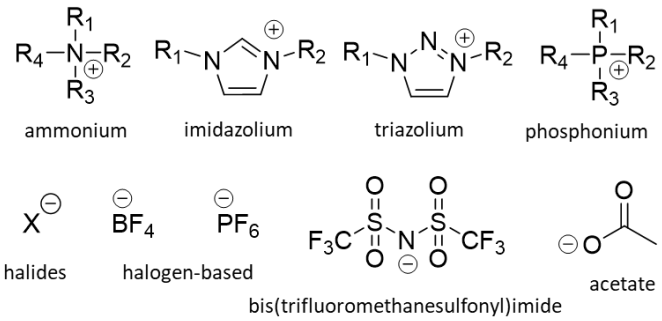

Figure 1. Examples of common ions used in ILs.

1.1.2 ILs with LC phases and plastic crystals

Condensed matter can be classified on the basis of the degree of order of its components (**Figure 2**). Crystalline solids possess long-range and three-dimensional order while being contraposed to isotropic liquids, which display an absence of positional and orientational long-range order. However, several materials (such as ILs) can be found in states with degrees of order which are intermediate between these two opposite cases. For this reason, they fall in the category of mesophases (from the Greek term *mesos*, meaning *between*, *middle*). These have been considered the "fourth state" of matter (in addition to

crystalline solid, liquid, and gaseous states)[18–21] and they can be further divided into multiple categories. Mesophases can be divided into three groups: LC (mentioned in the previous paragraph), plastic crystals, and conformational disordered crystals. The latter will not be taken into consideration in this work and, for this reason, it has not been included in **Figure 2**. It is relevant to highlight that the materials presented in this thesis are defined as thermotropic, meaning that their phase transitions are dictated by temperature change rather than concentration (lyotropic materials). Thus, all the considerations on mesophases are restricted to thermotropic cases.

The least ordered LC mesophase is the nematic phase, in which the molecules present only orientational order. In this state, the molecules generally align along a common direction, called the director.[22] Other LC mesophases with higher levels of order are achieved once the molecules retain a positional order in addition to the orientational one. These mesophases additionally organize in layered sheets (one-dimensional positional order) and they are divided into smectic A (SmA) and smectic C (SmC), depending on the director orientation: perpendicular to the sheets (SmA), or angled (SmC).[22,23] The degree of positional order can be then increased to a two-dimensional level with a columnar organization. These phases are promoted by molecules with disk-like shapes, rather than rod-like. For this reason, these can also be called discotic phases.[24]

Plastic crystals demonstrate higher order than LC and when ionic they have been referred to as "cousins" of ILs.[25,26] Plastic crystals are characterized by maintaining the centers of gravity for the constituting molecules fixed in space like in a crystalline structure, with long-range order, while achieving high vibrational and rotational freedom at short range. They usually exhibit one or multiple solid-solid phase transitions, which correspond to the activation of different molecular motions. Thus, once these materials reach their melting temperature (which is relatively low when compared to crystalline solids), the entropy is sufficiently high to lead to a low entropy of fusion ΔS_f (<20 $J \cdot K^{-1} \cdot mol^{-1}$ for neutral molecules and <60 $J \cdot K^{-1} \cdot mol^{-1}$ for ionic materials).[27,28] Due to their properties, which are very similar to those of ILs, ionic plastic crystals have seen high potential as solid ion conductors in solar cells, fuel cells, and lithium batteries.[26]

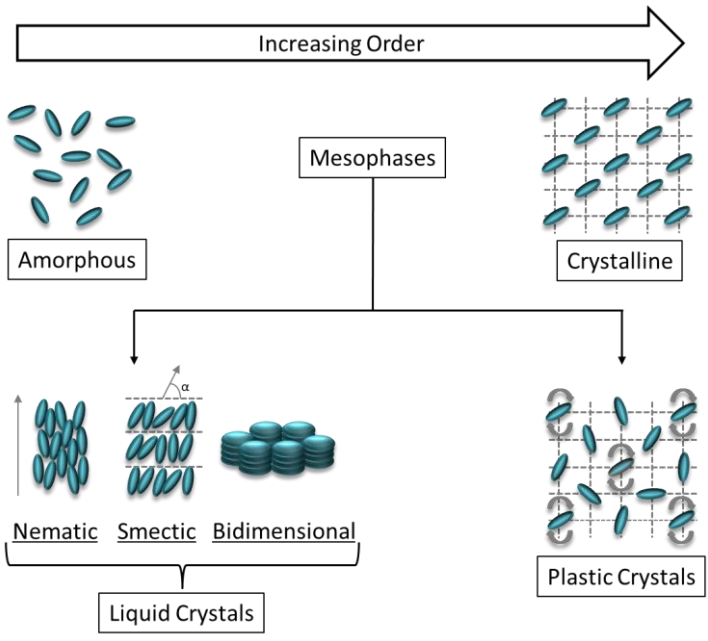

Figure 2. Order of hierarchy of some of the states of condensed matter.

1.2 Light and Materials

The topics collected in this sub-chapter focus on light-related concepts and phenomena that are relevant to the wide array of materials discussed in this thesis work. The first five sections will expose the background for light-emitting devices and preliminary concepts for the studied materials, while the last two paragraphs will respectively focus on *cis-trans* photoisomerization and the basis for harvesting solar energy *via* dye-sensitized solar cells (DSSCs).

1.2.1 Light-emitting devices

The field of light-emitting devices has received increasing attention over the past decades. Indeed, one of the viable strategies to tackle the enormous amount of electric energy demand relies on more efficient lighting technologies. Phones, computers, light bulbs, televisions, or anything that requires a digital interface have been and are continuously utilized for everyday life. For this reason, to make this consumption of electricity more economically and energetically bearable, two innovative devices have been the focus of research in the field. The organic light-emitting diodes (OLEDs) were the first to be

introduced in the academic world[29,30] and have recently seen commercialization in the wide market, while the light-emitting cells (LECs) were proposed later[31] and are still prerogative of academic research. LECs have been seen as competitors of OLEDs for their simple design. While OLEDs rely on a multilayered structure often composed of air-sensitive materials,[32] LECs require only one active layer, which is simultaneously acting as the emitter and charge transporter (**Figure 3**) and is sandwiched between two air-stable electrodes. This makes them cheaper and easier to manufacture than the OLEDs.

To achieve electroluminescence, the OLEDs working mechanism is based on the injection of electrons into the lowest unoccupied molecular orbital (LUMO) of the organic material and holes into the highest occupied molecular orbital (HOMO) after the application of external potential. The separated charges then drift under the action of the electric field, hopping from molecule to molecule, until they meet. Charge recombination then occurs through the formation of an excited state of the involved molecule (exciton), which then relaxes to the ground level with photon emission.[33] The LECs, instead, depend on the gradient of potential generated by the displacing of mobile ions under the application of a bias. The redistribution of ions forms *p* and *n*-doped regions at the opposite sides of the cell. Charges are then injected from the electrodes, before recombining in the middle of the active layer.[31]

In the last decades, several strategies have been explored and different materials have been investigated as light-emitting components for LECs [34,35] and the nature of the emitters advanced from conjugated polymers,[36–39] to ionic transition metal complexes (iTMCs),[40–44] to, most recently, quantum dots,[45–50] and small molecules.[51–55]

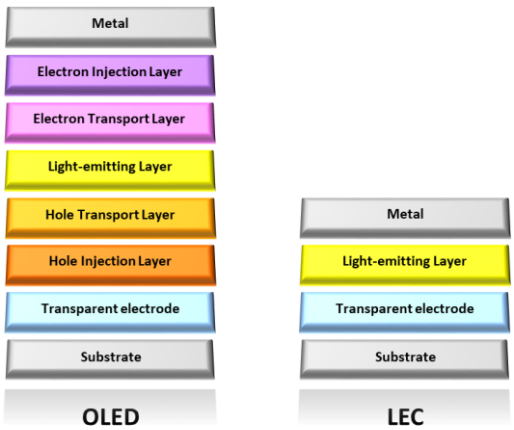

Figure 3. Schematic representation of OLEDs and LECs devices.

1.2.2 The rise and struggle of iTMCs

Polymer-based LECs require additional salts and ion-conductive polymers, other than the emissive material to achieve a proper and stable charge injection. To simplify the composition of the emissive layer, iTMCs were introduced.[56] Their ionic nature would make unnecessary additional salts and ion-conductive materials, being also suitable for solution processing. Furthermore, iTMCs proved to have better electroluminescent performances, due to their phosphorescent character.[57] The efficient luminescence is the result of the heavy atom effect of high atomic number transition metals. Heavy elements are characterized by strong spin-orbit coupling, which enables the radiative deactivation process from the triplet state, otherwise forbidden by selection rules.[58,59] This is a very important principle since 75% of excitons generated in an electrochemical device are triplets.[60–63] In order to harvest the energy related to the triplets, most of the studied iTMCs are based on metals that can exhibit a relevant heavy atom effect, such as ruthenium, platinum, and iridium. Unfortunately, these metals are expensive and rare, making their potential application in devices of everyday use unlikable, even if studies have been conducted to make materials adopting them as efficient as possible.[35,64–71] Therefore, materials involving inexpensive and more earth-abundant metals, such as copper and manganese,[72–74] or full organic materials have been increasingly studied over the last years, especially in the field of small molecules (SMs).[69,75]

1.2.3 Zero-dimensional hybrid organic-inorganic perovskites (HOIPs) and Mn(II)-emitters

One of the most efficient designs that have been used as a fundament for more earth-abundant light-emitting materials is the host-guest design.[76] This has found its best expression in the zero-dimensional hybrid organic-inorganic perovskites (HOIPs). Their structure is presented in **Figure 4**. Their working principle consists in treating the inorganic light-emitting units as doping agents inside an inert organic host matrix. HOIPs have several benefits, such as reduced self-absorption and self-quenching phenomena because of the long distances between the emitting centers, and allowing tunability of the luminescence properties through tailoring of the organic host molecules or the ligands.

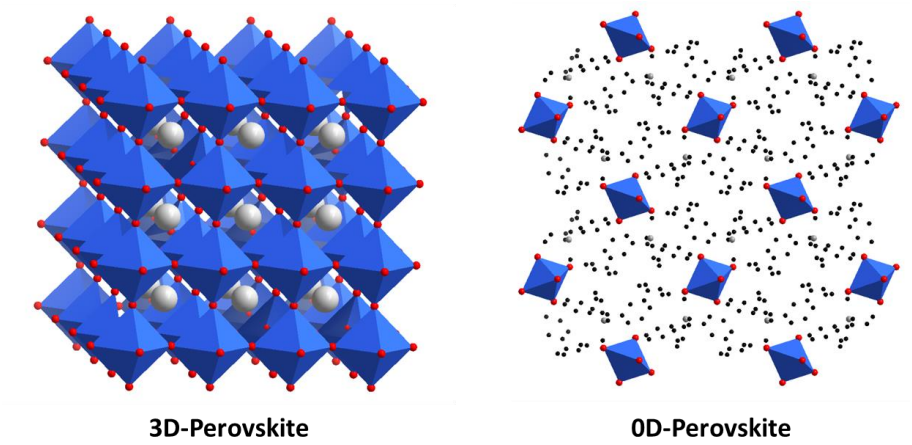

Figure 4. Comparison between three-dimensional (*left*) and zero-dimensional (*right*) perovskite structures.

In our modern world, there has been increasing attention to developing materials that have a minimal, if not absent, effect on the environment. The field of innovative luminescence is no exception. Even if research on lead-based HOIPs is still ongoing, their instability and toxicity have always been an issue to address.[77,78] Thereby, less toxic and lighter elements of the first row of transition metals have also been recently studied in HOIPs and have demonstrated extremely good luminescence in this type of structure.[79] In our studies, we took into consideration the earth-abundant manganese(II) bromide complexes as the light-emitting units, allowing us to explore the green and red regions of the visible spectrum.

Mn(II) complexes have been broadly investigated because of their peculiar phosphorescent behavior. Their luminescence is the result of radiative deactivation from the $^4T_1$ state to the $^6A_1$ ground state, a d-d transition closely related to the crystal field strength and, therefore, to the nature of the ligands and the coordination geometry.[73,80–86] In simple terms, the generally observed trend shows that octahedral coordination of the Mn(II) center leads to red light emission, while tetragonal coordination yields green light (**Figure 5**). Interestingly, halide salts of Mn(II) have demonstrated the ability to switch from octahedra to tetrahedra if exposed to heat, while the opposite process could occur only after solubilization and recrystallization. In contrast to this behavior, a series of ionic materials have shown the potential to reversibly interchange between the two configurations of the Mn(II) halide complexes.[87,88] In one case, this was observed to take place together with the phase transition from crystalline solid to mesophase and *vice-versa*. In the mesophase state, the Mn(II) tetrahe-

dra come in contact to form polymeric chains of octahedra through face-sharing, allowing, therefore, the photoluminescence to switch from green to red. In the second case, the geometry conversion was associated with the presence of coordinating water molecules, which would be released upon heating allowing the geometry of the complex to switch from octahedral to tetrahedral. Upon cooling in air, water molecules would be reabsorbed, resulting in a structural change with the restoration of the octahedral coordination.

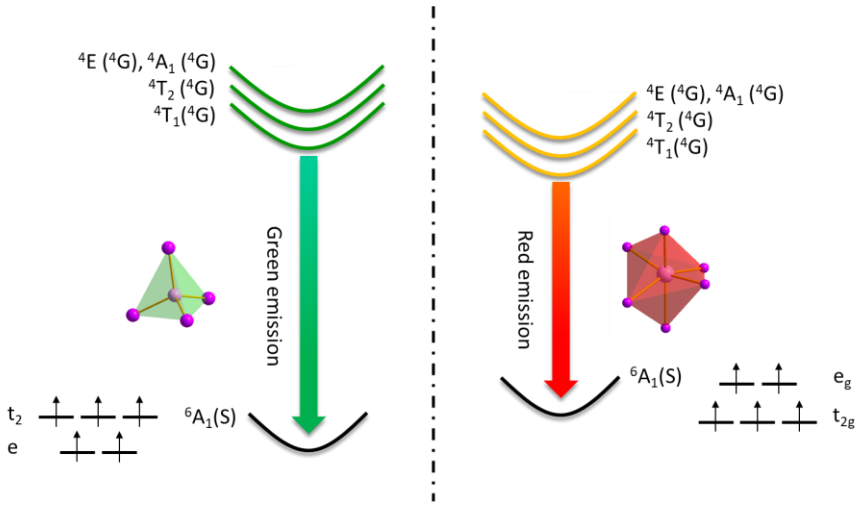

Figure 5. Energy diagram for the emission of Mn(II) complexes in tetrahedral (*left*) or octahedral (*right*) complexes (high spin configuration).

1.2.4 Phosphonium cations for Mn(II) HOIPs

The organic cations in HOIPs have multiple roles. They are fundamental for ensuring the rigidity of the structure and the isolation of the emitting centers, allowing efficient luminescence. Additionally, their functionalization with aryl groups can lead to the antenna effect and therefore energy transfer to the inorganic emitting center. Promising results were obtained with phosphonium cations, more specifically the tetraphenylphosphonium $[Ph_4P]^+$. The most relevant example is the recently reported green-emitting tetraphenylphosphonium tetrabromidomanganate(II) $[PPh_4]_2[MnBr_4]$.[89] These ionic materials have demonstrated high and efficient luminescence with quantum yield (QY) up to unity and have also been used together in a sunlike OLED.[90] Being the inorganic anions isolated and surrounded by rigid cations, the self-quenching of the excited state is hindered, leading to the reported performances.[82,91] Similar materials could also find applications in LECs. Nevertheless, the high tendency to crystallize demonstrated by these materials

would create issues while building the device (*i.e.* irregular distribution of the material and formation of boundaries that can obstacle the transport of charges), leading to poor performances. To address this problem, in Paper I and Paper II we looked at the design principles of ILs and the prepared materials will be discussed in the main body of this thesis work.

1.2.5 SMs and 8-Hydroxyquinolines as extremely compact emitters

Another of the possible strategies previously mentioned for low-cost light-emitting materials is based on SMs.[69,92] The research on this class of materials found fertile soil especially in the field of blue-light emission,[93,94] since they tend to not incur in self-destruction mechanism characteristic for iridium complexes or organic polymers.[95,96] The SMs normally rely on extended delocalized organic systems rather than emitting metals.[93,94] The nature of SMs can be either ionic[97] or neutral (therefore requiring to be blended with an additional conducting material).[98] Ionic SMs revealed overall higher performances than the neutral ones when applied in light-emitting devices.[69] Nevertheless, the synthetic procedure for these SMs is generally complex, making production more challenging.

In our look for economic and synthetically accessible blue emitters, we found a promising candidate in the 8-hydroxyquinolines (8Hqs) series, which inspired the work presented in Paper III. 8Hqs are very simple SM emitters whose promising properties have been demonstrated when applied in OLEDs.[99–102] More specifically, the complex tris(8-quinolinato)aluminum (Alq_3), first reported in 1987 (**Figure 6**),[103] has revealed green-blue emission rising from the organic ligand, drawing the attention of the scientific community. It has been found that the luminescence of 8Hq is easily tuned through its functionalization with electron-donating or electron-withdrawing groups. This is due to the localization of the HOMO and the LUMO on the phenolic and pyridinic rings, respectively.

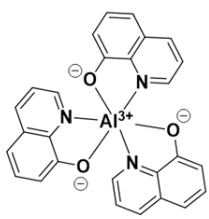

Alq_3

Figure 6. Molecular structure of the Alq_3 complex.

Nevertheless, studies of 8Hq in solution demonstrated its weak fluorescence because of fast proton transfer deactivation of the excited state.[104–106] This mechanism has been identified for both cationic and anionic forms, but higher photoemission QYs could be achieved in strong acidic or basic conditions.[106,107] In the case of Alq_3, this quenching process is prevented, resulting in high QYs and suitability in electroluminescent devices.

1.2.6 Azobenzene photoisomerization

Light is the most relevant source of energy for all living organisms. Radiative energy is collected and stored as high-energy chemicals, which are then utilized for the needed biological functions.[108] During these processes, the high-energy chemicals act as "fuel". The obtained products are "waste", molecules that are not needed anymore and have to be removed to allow the correct operation of the system. Nevertheless, some chemicals do not generate side species, but they undergo clean and reversible processes. Examples of this kind of compounds are the azobenzenes (**Figure 7**).[109] Light excitation of this class of molecules leads to *cis-trans* photoisomerization via in-plane inversion or twisting around the N=N double bond.[110,111] Due to the reversibility of the process, azobenzenes have been widely studied, ranging from application in the fields of data storage[112] and optical switching[113] to being reported as a base for light-driven molecular machines.[114]

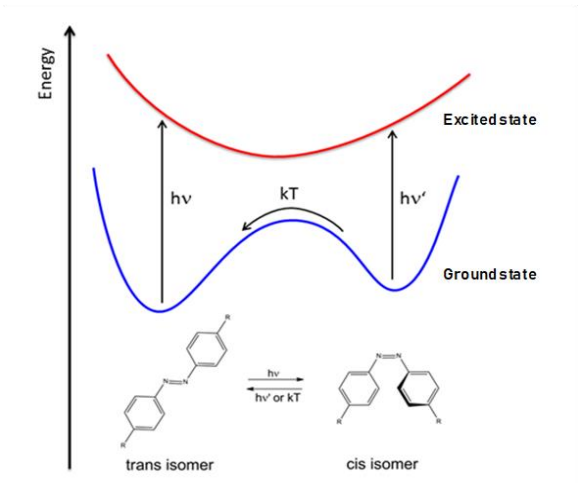

Figure 7. Energy profile for the *cis-trans* isomerization of azobenzenes, where h is the Planck's constant, ν and ν' the frequency of the photons exciting respectively the *trans* and the *cis* isomers, k the Boltzmann's constant, and T the temperature (Adapted with permission from Paper IV).

1.2.7 Importance of Solar Energy and ILs in Dye-Sensitized Solar Cells (DSSCs)

Light can not only be used for the aforementioned chemical processes, but also for electrical energy production. In our growing modern world, the global energy demand has been constantly rising. Only in the past years, the outbreak of the disease COVID-19 led to a drop that has not been seen in the last 70 years.[115] The effects of lockdowns and social distancing on the population have influenced the energy management of industry and households, revealing the challenges and the consequent opportunities for post-pandemic recovery.[116] One of the opportunities would be the investment in renewable energy,[117] especially since providers of wind- and solar-generated electricity have not seen detrimental slowdowns.[115] Even before the appearance of COVID-19, photovoltaic energy and solar cells drew researchers' attention since harvesting the amount of solar radiation hitting the Earth for just one hour ($4.3 \cdot 10^{20}$ J) would be sufficient to satisfy the world energy demand of one year ($4.1 \cdot 10^{20}$ J).[118]

DSSCs have been demonstrated to be a valid alternative to semiconductor-based solar cells, due to their lower production cost, flexibility, and promising efficiencies that bode well to reach the Shockley-Queisser limit of 33%.[119] Their design requires a light-harvesting anode normally based on TiO_2 and a dye separated from the poly(3,4-ethylenedioxythiophene) polystyrene sulfonate (PEDOT:PSS) cathode by an electrolyte solution. The two electrodes are then connected externally through a circuit, therefore generating current that can be used for energy storage (**Figure 8**). The lifetime of these devices is strongly affected by the electrolyte intermediate responsible for the charge equilibrium. The most applied electrolyte in DSSC is the redox couple I^-/I_3^-, which normally requires the presence of a solvent and has been shown to lead to corrosion of the metal electrodes, among other drawbacks.[120] The utilization of a solvent (*e. g.* ethanol, acetonitrile, DMSO) brings obvious limitations due to its intrinsic volatility, especially when the DSSC is operated for a long time and at high working temperatures.[121]

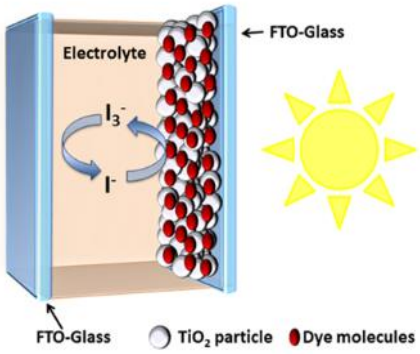

Figure 8. Schematic overview of the operating principle of a DSSC (Adapted with permission from Paper V). FTO-glass stands for fluorine-doped tin oxide-glass.

ILs have strongly demonstrated their suitability for the substitution of electrolyte media, thanks to their almost negligible vapor pressure, high thermal and chemical, and electrochemical stability.[122–126] These properties often come together with high viscosity, which hinders the movement of the charges affecting negatively the performance of the cell.[127,128] This obstacle has been shown to be bypassed by ILs presenting an LC mesophase.[129–131] Due to the ability to form such phases, these materials can form a two-dimensional electron-conductive structure between the electrodes.[130] This abated the resistance to the charge movement, thus improving the photocurrent density and leading to well-performing DSSCs.

1.3 Scope of the thesis

This thesis was inspired by the high versatility and peculiar physicochemical properties of ILs. The target of this work was to explore the suitability of ILs and materials inspired by ILs for light-related applications.

2. Preparation and characterization of materials

This chapter includes the procedures for the preparation of materials and a brief description of the analysis techniques utilized. More details are provided within the attached Papers from I to V.

2.1 Preparation of materials

2.1.1 Synthesis of ILs and ILs-inspired materials

The synthetic procedures utilized for all the ILs and ILs-inspired materials reported in the manuscripts collected in this thesis follow a simple double-step reaction as a basic procedure (**Figure 9**). The first step normally involves the functionalization of alkyl- or aryl-phosphine in Papers I and II, of 8-hydroxyquinoline in Paper III, and of imidazole or triazole in Papers IV and V. For Papers I-III this allowed obtaining the cations of interest. The second step consists of the metathesis of the anion, the exchange of the counterion of the cation obtained in the first step with the desired one, for the materials presented in Papers I-III. In Papers I and II, this step is associated with the halide complexation of Mn(II). For Papers IV and V, the second step is related to a second functionalization of the imidazole or triazole and the formation of the cation of interest. When possible, the synthesis is followed by extraction to increase the purity of the final product. Subsequently, the final material is dried under a dynamic vacuum. Each cation would need specific working conditions such as solvents and temperatures. Due to the sensitivity of the reagents and products to exposure to oxygen and moisture present in the air, some of the reactions need to be performed under an inert atmosphere (i.e. glovebox and Schlenk techniques) and with dry solvents. More details can be found in the respective papers.

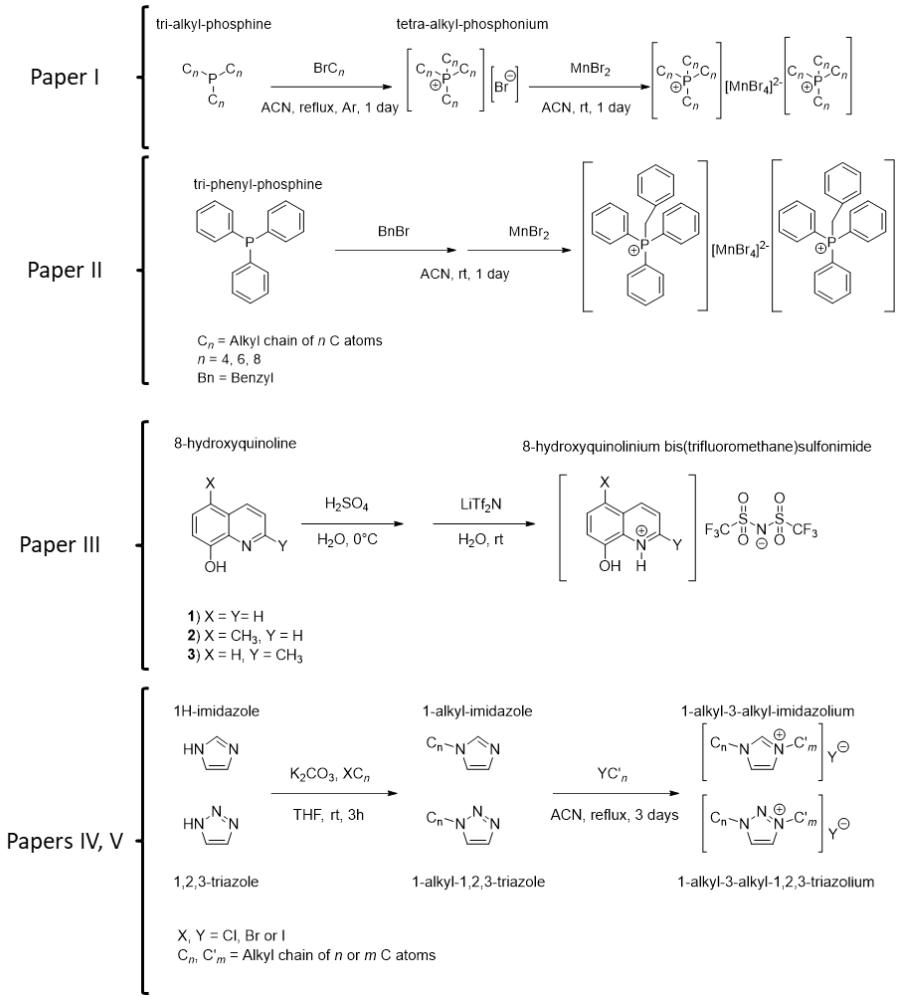

Figure 9. Two-step synthesis of the materials presented in this thesis.

2.2 Methods and Analysis Techniques

2.2.1 Cyclic Voltammetry (CV)

CV is a versatile electrochemical technique where the potential of a working electrode (WE) is cycled within a predetermined potential range and the resulting current is recorded. In correspondence with electrochemical processes such as reduction and oxidation of the investigated species or the utilized media, the absolute current signal will increase non-linearly with the potential trend. Two possible setups are available: two-electrode or three-electrodes system. In the first one, only the WE and reference electrode (RE, used to determine the potential on the WE) are utilized. In the second system, an additional counter electrode (CE) is used. The CE function is to avoid high currents running through the RE, risking to affect its potential.

In this thesis work, the CV has been utilized mainly to establish or have insight into the electrochemical stability and HOMO-LUMO gap of the investigated proposed materials. Different setups for the cyclic voltammetry were used for the manuscripts presented herein. Nevertheless, all of them were recorded on the same Gamry Instrument Interface 1010 potentiostat (Gamry Instrument, Warminster, PA) applying a three-electrode system. For all the cases, solutions between 10^{-4} M and 10^{-3} M of the investigated salt were prepared and transferred into the cell. Salts such as $LiTf_2N$ or $LiClO_4$ were added to the solutions to increase the conductivity. Additionally, the measurements were performed while holding the cell under Ar if not differently specified. In **Figure 10**, a schematic representation of the utilized three-electrode system is provided.

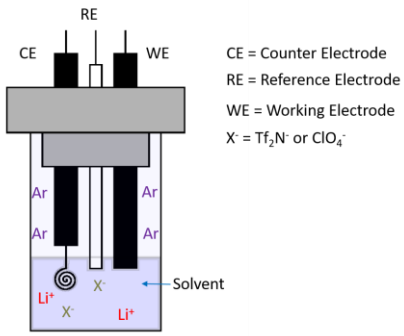

Figure 10. Schematic representation of the setup utilized for cyclic voltammetry measurements.

2.2.2 Crystal Growth

Crystals suitable for structural characterization were grown, when possible, by isothermal evaporation. The desired IL or salt was dissolved in a solvent with high vapor pressure to form dilute solutions. The so obtained solution was then let in the open air, giving enough time for the solution to yield nuclei for crystal formation.

2.2.3 Differential Scanning Calorimetry (DSC)

DSC allows for the identification of endo- and exothermic processes which a sample undergoes as a consequence of temperature variation. The obtained data can be plotted in curves that were used in this thesis work to recognize specific phase transitions such as solid-solid transitions, crystallization, melting to isotropic liquid or mesophases, and vitrification. Additionally, analyses of all but the latter-mentioned phenomena (second-order transition) allow for the calculation of the associated enthalpy and entropy. The last one was revealed to be a key element for the identification of the nature of specific mesophases.

The majority of the DSC measurements were performed with a computer-controlled Phoenix DSC 204 F1 thermal analyzer (Netzsch, Selb, Germany). Measurements were carried out at a heating rate of 1 $°C \cdot min^{-1}$ or 5 $°C \cdot min^{-1}$ with a nitrogen flow rate of 40 $mL \cdot min^{-1}$. The samples were placed in aluminum pans which were cold-sealed and punctured if the sample was air-stable.

2.2.4 Infrared Spectroscopy (IR)

The spectra obtained *via* IR allow probing of the vibrational modes (such as stretching and bending) of materials. Here, IR was used mainly as a complementary technique to nuclear magnetic resonance (NMR, see further) and mass spectrometry (MS, see further) for the identification of characteristic modes for the starting materials and the synthesized products or solvent residues.

IR data were collected on a Bruker Alpha-P ATR-spectrometer equipped with a diamond crystal (Karlsruhe, Germany) in an attenuated total reflection configuration. The obtained spectra were then processed with the OPUS program (Bruker, Ettlingen, Germany).

2.2.5 Karl Fischer Titration

The Karl Fischer titration is a well-established method to evaluate the water content (in the order of ppm) of a substance. This technique is employed especially for materials that seek application in electrochemical devices such as batteries since the presence of water would be detrimental to the longevity of the apparatus. The base principle relies on the reaction:

$$2\,H_2O + SO_2 + I_2 \rightarrow H_2SO_4 + 2\,HI$$

in which one molar equivalent of iodine and one molar equivalent of water are consumed. In this thesis work, this technique was adopted to assess the amount of water for ionic materials which synthetic procedure was carried out without a protective atmosphere nor dry solvent and which IR spectra did not show the clear presence of water.

The Karl Fischer titration measurements were carried out following with a C10S KF Coulometer (Mettler Toledo, Sweden).

2.2.5 Mass Spectrometry (MS)

MS is a technique that is founded on the ionization of the investigated materials. The latter can break into ionic fragments (or just become ionized) that are then separated and recorded according to their mass-to-charge ratio with the aid of magnetic or electric fields. This technique was utilized as a complementary analysis for the identification of the desired final materials.

An SYNAPT G2-S HDMS Q-ToF Mass Spectrometer (Waters, Manchester, UK) with an electron spray ionization (ESI) operated in the positive and negative ion mode, was used. The ion source was set up as follows: capillary voltage: 2500 V, extractor: 1.0 V, RF lens: 0.5 V, ion source temperature: 120 °C, and desolvation temperature 250 °C. N_2 was used as both the cone and desolvation gas at a flow of 70 L/h and 500 L/h, respectively. Ar was used as collision gas at a pressure of $2.95 \cdot 10^{-4}$ mbar. The detector was a time-of-flight (TOF).

2.2.6 Nuclear Magnetic Resonance (NMR)

NMR is a well-known technique in organic chemistry for the determination of the structure of molecules in deuterated solutions (*i.e.* D_2O, d-DMSO,

$CDCl_3$) or even in solid states. In the presented work, NMR has been used (when possible) to determine the purity of the synthesized materials.

Characterization through ^{1}H-, ^{13}C-, and ^{31}P-NMR was performed at room temperature on a Bruker 400 MHz spectrometer equipped with a broadband observe (BBO) probe (Bruker AXS, Karlsruhe, Germany). ^{19}F-NMR spectra were recorded at room temperature in DMSO on a Bruker 400 MHz Ultrashield spectrometer equipped with a BBO probe (Postdam, Germany). The identified peaks were reported with chemical shifts (δ units) expressed in ppm. The solvents used were $CDCl_3$ or d_6-DMSO, and the chemical shifts of the ^{1}H-NMR spectra were reported with respect to residual solvent signals, which are specified within each manuscript.

2.2.7 Photoluminescence Characterization

The mechanism of emission of luminescent materials and their efficiency can be investigated by the recording of excitation and emission spectra. The former are obtained while scanning excitation wavelength (λ_{ex}) and recording how the luminescence at a fixed wavelength (λ_{em}) increases or decreases in intensity. The resulting spectra reveal the energy bands that lead to the light emission. The emission spectra are obtained when exciting with a fixed λ_{ex} and checking the observed intensity at different λ_{em}. These give objective information on the emission energy (non-biased by the human eye). The efficiency of the luminescence or quantum yield (QY) is calculated utilizing the reflectivity and the emission of both the sample and a blank (high reflectivity, low emission), normally $BaSO_4$. The lifetime of emitters is investigated by exciting with a pulsed laser (fluorescence investigation) or a pulsed discharge lamp (phosphorescence investigation) and recording the time between the exciting photon of the source and the emitted photons of the luminescent materials.

The luminescent materials were characterized by collecting steady-state excitation and emission spectra, the lifetime of the excited state, and the quantum yield on a HORIBA Jobin Yvon FluoroLog-3 modular spectrofluorometer with an R928P PMT detector (Horiba France, Longjumeau, France).

2.2.8 Powder X-Ray Diffraction (PXRD)

PXRD is a technique that utilizes X-rays to analyze the crystalline nature of powder samples. In this work, the PXRD has been used to verify the phase purity of materials whose structure was identified with single crystal X-ray

diffraction (see below) and to observe the accomplishment of phase transitions (vitrification, solid-solid).

Diffraction data on powders were collected at room temperature on a PANalytical X'pert PRO diffractometer (Malvern Panalytical, Malvern, United Kingdom) using CuKa1 radiation in reflection mode. The diffraction patterns were collected in the 2θ range 5°–70°. For X-ray fluorescent compounds, PXRDs were collected on a Bruker Phaser D2 diffractometer using CuKα radiation in reflection mode. The instruments were operating at 45kV and 40 mA and with a rate of 0.55 sec/step.

2.2.9 Raman Spectroscopy

Raman spectroscopy, similarly to IR, is used to identify vibrational modes in the investigated materials. However, some of these modes are active and therefore can be probed only in one of the two techniques. For the results presented in this thesis, Raman spectroscopy was utilized to confirm the coordination geometry of $[MnBr_4]^{2-}$ complexes.

Raman Spectroscopy measurements were performed at room temperature using a Horiba LabRAMHR system (Horiba Europe, Sweden) equipped with a red laser (λ = 785 nm) and a CCD detector. The instrument was calibrated with a Si standard.

2.2.10 Single Crystal X-Ray Diffraction (SCXRD)

SCXRD is one of the most utilized methods to determine the crystal structure of a crystalline material. Similarly to the PXRD, X-rays are used to generate a pattern of reflections which can be then traced back to the crystalline structure. Herein, this technique was used to obtain precise information regarding the configuration of the ionic moieties, allowing us to have a deep understanding of the material properties.

Structural characterization of crystalline compounds was performed on different single-crystal X-ray diffractometers, using Kα radiation of Cu or Mo at different temperatures, from 100 K to room temperature. The diffractometers utilized were a Stoe IPDS-I, a Bruker D8 Venture, and an Agilent SuperNova.

2.2.11 Thermogravimetry Analisis (TGA)

TGA consists in recording the weight change that occurs while heating a known amount of sample. This allows for identifying the presence of solvents, which evaporation will be recorded as a weight loss, providing insight into the decomposition process (in an inert atmosphere), or tracing oxidation of the material while in an unprotected atmosphere. In this thesis work, this technique was used always in inert conditions.

TGA measurements were performed with a TG 449 F3 Jupiter (Netzsch, Selb, Germany). Measurements were carried out in aluminum oxide crucibles with a heating rate of 10 °Cmin-1 and N_2 or Ar as the purge gas. Onset values are given as defined by 5% weight loss.

2.2.12 UV-Vis Absorption

Light absorption can be explained following the empirical Lambert-Beer law

$$A = \epsilon l C = log_{10}(I_0/I)$$

with A absorbance, ϵ molar extinction coefficient, *l* length of the optical path, *C* concentration of the investigated solution, I_0 the intensity of the light source irradiating the sample, and *I* the intensity of the light not absorbed from the sample and reaching the detector. In the case of a solid sample, the same information can be obtained by recording the intensity of the light reflected by the material and following the relationship

$$A = -log_{10}R$$

where *R* is the intensity of the reflected light. The calculation and plotting of this dimensionless property over the wavelength of the light source give insight into the energy bandgaps and levels of the investigated materials. This information can be used for several different applications. In this work, this type of analysis has been used to probe *in-solution* behavior of ionic materials, to observe isomerization, and as a complementary technique to the photoluminescence characterization.

Absorption spectra in the near UV and visible region of the light were recorded for solids, liquids, and solutions on an Agilent Technologies Cary 5000 UV-Vis-NIR spectrophotometer equipped with an Agilent Praying Mantis

diffuse reflectance accessory (Agilent Technologies, Kista, Sweden). Liquids and solutions were measured inside cuvettes of 1 cm light path.

3. Papers I-II: Luminescent manganese-containing ionic materials

Papers I and II collect studies on ionic materials sharing the same $[MnBr_4]^{2-}$ anion but with phosphonium-based cations functionalized in different ways. In Paper I, the design that was taken into consideration was focused on symmetric tetraalkylphosphonium cations. To investigate the effect of the chain length on the thermal and optical properties and with the purpose of finding a good balance between optical properties and IL-like processability, three different alkyl functions were studied: butyl (C_4), hexyl (C_6), and octyl (C_8). In Paper II, instead, the properties of the more rigid triphenylbenzylphosphonium $[Ph_3PBn]^+$ were explored. Its design is based on the introduction of an element of asymmetry, the benzyl (Bn) group, in the well-performing and previously mentioned $[PPh_4]_2[MnBr_4]$. This has been recently achieved by Qin and collaborators,[132] who synthesized the bis-triphenylbenzylphosphonium tetrabromidomanganate $[Ph_3PBn]_2[MnBr_4]$. In their study, a series of Mn(II)-based compounds is presented, with a brief characterization for each of them. This consisted of TGA up to 650 °C, crystal structure, photoluminescence, and triboluminescence studies. Since the cations bear three phenyl rings and one benzyl unit, we expected the ionic material to show reduced rigidity and crystallinity (compared to $[PPh_4]_2[MnBr_4]$). These are qualities that would suit well for application in LEC since they could allow for better ion conduction. For this reason, we decided to expand the thermal characterization of $[Ph_3PBn]_2[MnBr_4]$ and to study the performances of LEC adapting it as a guest emitter.

3.1 Mesophase formation and structural characterization

The compounds bis-tetrabutylphosphonium tetrabromidomanganate $[P_{4444}]_2[MnBr_4]$ and bis-tetraexylphosphonium tetrabromidomanganate $[P_{6666}]_2[MnBr_4]$ were obtained as waxy light yellow powders, while the bis-tetraoctylphosphonium tetrabromidomanganate $[P_{8888}]_2[MnBr_4]$ was collected as a dark yellow-orange oil. These first qualitative observations already pointed toward non-crystalline behavior and the tendency to form mesophases. $[Ph_3PBn]_2[MnBr_4]$, on the other hand, was obtained as a whitish powder. Thermal analysis with DSC (**Figure 11**) paired with POM (**Figure 12**) unveiled the IL-like behavior of $[P_{4444}]_2[MnBr_4]$ and $[P_{8888}]_2[MnBr_4]$, while $[P_{6666}]_2[MnBr_4]$ and $[Ph_3PBn]_2[MnBr_4]$ did not fit into the category due to their high melting point (over 200 °C). While $[P_{8888}]_2[MnBr_4]$ maintained the liquid state all over the investigated temperature range (thus getting classified as room temperature IL (RTIL)), $[P_{4444}]_2[MnBr_4]$, $[P_{6666}]_2[MnBr_4]$, and $[Ph_3PBn]_2[MnBr_4]$ exhibited multiple phase transitions, as revealed by the heat-exchange profiles.

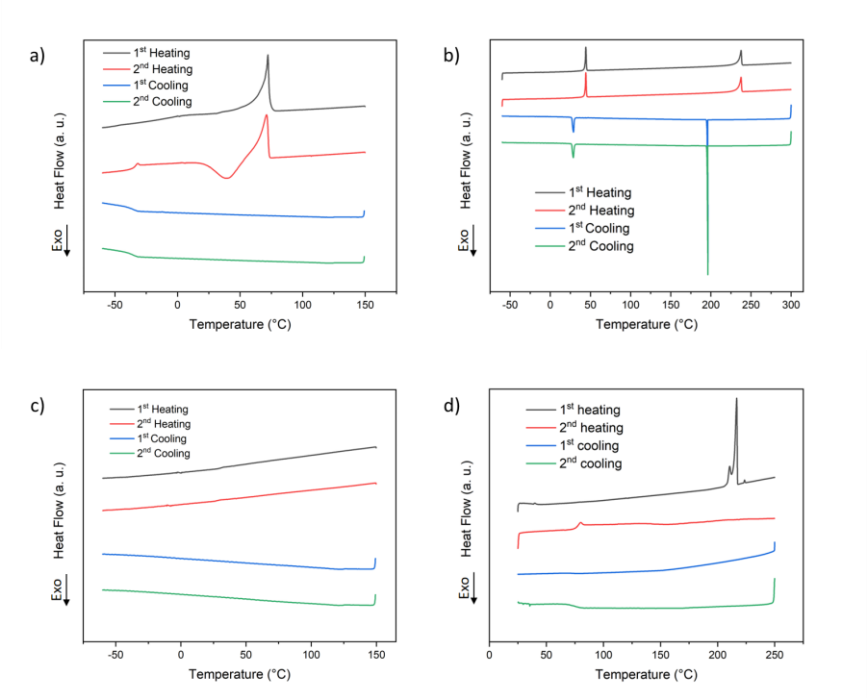

Figure 11. DSC curves for compounds $[P_{4444}]_2[MnBr_4]$ (a), $[P_{6666}]_2[MnBr_4]$ (b), $[P_{8888}]_2[MnBr_4]$ (c), and $[Ph_3PBn]_2[MnBr_4]$ (d).

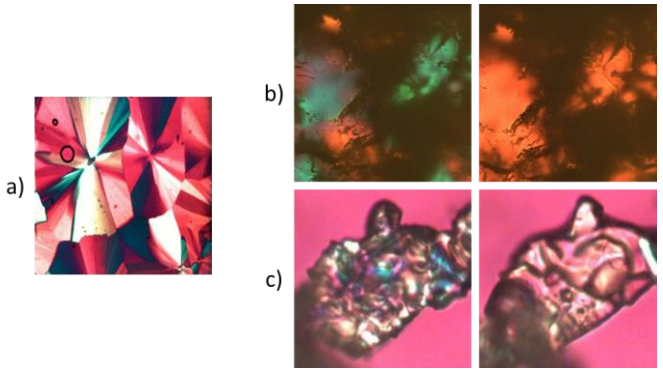

Figure 12. a) Conical feature of the SmA mesophase of $[P_{4444}]_2[MnBr_4]$; b) difference of light diffraction between the LTS (*left*) and the HTS (*right*) of $[P_{6666}]_2[MnBr_4]$; c) polycrystalline phase (*left*) and unidentified mesophase (*right*) of $[Ph_3PBn]_2[MnBr_4]$.

$[P_{4444}]_2[MnBr_4]$ showed a melting point of 68.4 °C upon the first heating ramp and glass formation at T_g = -34 °C upon the first cooling cycle. The molten state was recovered in the second heating cycle upon reaching approximately the same T_g. Continuing to increase the temperature (second heating ramp) an exothermic process with an onset at 22.0 °C to a SmA phase was identified due to the appearance of conical features in POM (**Figure 12a**), before melting occurred at 67.9 °C.

During all the heating ramps, $[P_{6666}]_2[MnBr_4]$ transitioned endothermically from a low-temperature solid phase (LTS) to a high-temperature solid phase (HTS) at 43.1 °C and then melted at 234.5 °C. The cooling cycles displayed the two reverse processes, being the transition to the HTS from the molten state at 196.2 °C and the conversion to the LTS at 30.2 °C. When analyzed with POM (**Figure 12b**), the solid-solid transition was detectable as a change of the light diffraction, from displaying different colors in the LTS to not showing any (absence of diffraction) in the HTS. Interestingly, the melting transition was accompanied by a small entropy change (22 $J\ K^{-1}\ mol^{-1}$) for a non-IL compound, especially when compared to higher-temperature melting salts. The small value of the entropy of melting, along with the results of the crystal structural characterization, is important for the understanding of the underlying mechanism of the phase transformation, as will be discussed below.

When heated to high temperatures (up to 250 °C), $[Ph_3PBn]_2[MnBr_4]$ exhibited three endothermic phase transitions. The first two occurred in a short

range of 13 °C, without being completely resolved even at a low heating rate (1 °C min^{-1}). Unfortunately, POM analyses (**Figure 12c**) did not allow unequivocal identification of the phases. During the first transition at 207 °C, the crystalline material most likely evolved to another crystalline phase, which could be speculated due to the polycrystallinity observed under the polarized light. This phase was then further converted to an unidentified mesophase at 214 °C before finally transitioning to isotropic liquid at 220 °C, which is indicated by the extremely low enthalpy associated with the transition. Interestingly, following cooling never restored a crystalline phase. Instead, near 77 °C the material underwent glass formation even when performing measurements with low cooling rates. Curiously, this is a thermal behavior that we have seen often related to ILs. It can be speculated that the reason for this behavior has to be connected to the benzyl group, which mobility in the liquid state could hinder the ability of the molecule to reorganize in a regular crystalline structure.

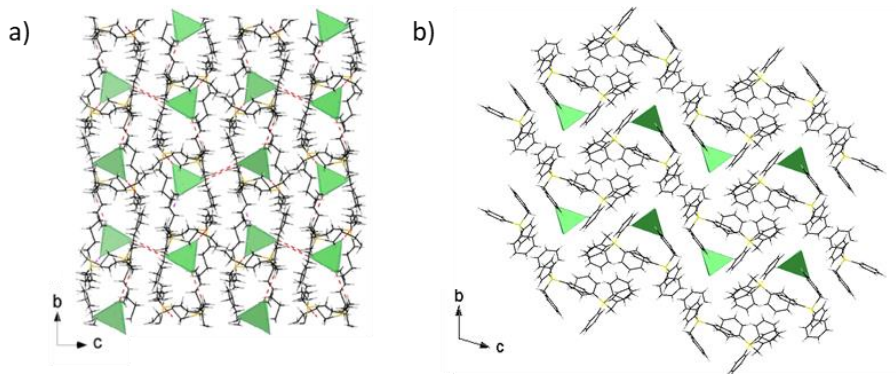

Figure 13. Projection of the crystal structure of $[P_{4444}]_2[MnBr_4]$ (a) and $[Ph_3PBn]_2[MnBr_4]$ (b) showing the distribution of the isolated $[MnBr_4]^{2-}$ complexes down the *a*-axis.

Only $[P_{4444}]_2[MnBr_4]$ and $[Ph_3PBn]_2[MnBr_4]$ were found to form crystals of sufficient quality for SCXRD analysis, revealing similar HOIP structures (**Figure 13**). In both cases, weak C-H---Br hydrogen bonds and hydrophobic interaction were found. These could account for the formation of not well-stabilized mesophases. Regarding $[P_{6666}]_2[MnBr_4]$, the obtained crystals gave very poor resolution at SCXRD (1.89 Å), allowing only the identification of the unit cell. The indexing of diffraction spots collected in temperature-dependent measurements yielded a face-centered cubic unit cell with a = 23.63(2) Å for the HTS. The same kind of measurements was conducted for the LTS, but the indexing of the diffraction peaks did not lead to a well-defined structure. More insight into the two solid phases was instead given from temperature-dependent PXRD studies. Indexing of the Bragg reflections

collected for the HTS (~50 °C) yielded a face-centered cubic unit cell with a = 23.623(3) Å, thus matching the result obtained from SCXRD. The PXRD pattern collected for the LTS was characterized by a higher number of peaks, which were indexed in a monoclinic unit cell with a = 28.130(1) Å, b = 17.224(6) Å, c = 28.627(1) Å, β = 110.561(2)°. Additionally, it was possible to find a transformation matrix from the unit cell of the HTS to the one of the LTS, therefore providing evidence that the two are structurally related. These results, together with the low entropy of melting, could indicate that $[P_{6666}]_2[MnBr_4]$ is a plastic crystal.

3.2 Photo- and electroluminescence of Mn(II)-emitters

The ionic materials containing $[MnBr_4]^{2-}$ anions exhibited an expectedly green photo- and electrostimulated emission (**Figure 14**). The emission was centered at 512 nm for $[Ph_3PBn]_2[MnBr_4]$, 520 nm for $[P_{4444}]_2[MnBr_4]$ and $[P_{6666}]_2[MnBr_4]$, and 530 nm for $[P_{8888}]_2[MnBr_4]$. Photoexcitation near 280 nm led to emission from the $^4T_1(G)$ state for all the compounds. While an antenna effect could be seen for the $[Ph_3PBn]_2[MnBr_4]$, the same could not be observed for the tetraalkylphosphonium due to the absence of aromatic groups on the cations. Instead, photoluminescence was still obtained when exciting at high energies due to the excitation to the $^4T_2(F)$ state of the manganese center. The same emission was obtained when exciting with a less energetic wavelength (361 nm), targeting the $^4T_2(D)$ state. While the emission of $[P_{8888}]_2[MnBr_4]$ was extremely weak, that of $[P_{4444}]_2[MnBr_4]$, $[P_{6666}]_2[MnBr_4]$ (LTS), and $[Ph_3PBn]_2[MnBr_4]$ was intense enough for lifetime and QY evaluation. When the luminescence of the HTS of $[P_{6666}]_2[MnBr_4]$ was recorded, the intensity decreased significantly, making the calculation of the lifetimes and the QY not possible.

The lifetimes were in the microsecond region for all the compounds, indicating the phosphorescent nature of the emission. The longest lifetime recorded at room temperature was 304 μsec for $[Ph_3PBn]_2[MnBr_4]$ when excited at 280 nm. When exciting at 276 nm, $[P_{4444}]_2[MnBr_4]$ showed a lifetime of 149.1 μsec and $[P_{6666}]_2[MnBr_4]$ (LTS) a lifetime of 134.7 μsec. At the longer wavelength of 361 nm, the lifetimes did not undergo dramatic variations, being respectively 301 μsec for $[Ph_3PBn]_2[MnBr_4]$, 149.7 μsec for $[P_{4444}]_2[MnBr_4]$, and 133.4 μsec for $[P_{6666}]_2[MnBr_4]$ (LTS). The decay of the excited states was fitted with mono-exponential curves, confirming the existence of only one singular type of emitting center.

While the QY of the $[Ph_3PBn]_2[MnBr_4]$ reached unity, the other compounds did not reach such high values. The $[P_{4444}]_2[MnBr_4]$ and the $[P_{6666}]_2[MnBr_4]$ (LTS) exhibited similar QYs, within the limit of the experimental error (~10%), being around 60%. This demonstrated that efficient luminescence can be obtained also without antenna groups. Similar results were already reported for compounds with tetraalkylammonium cations,[133] but there was no evidence of the performance of the phosphonium relatives, especially those functionalized with long alkyl chains.

Envisioning the application of our salt in light-emitting devices, we have checked the photoluminescence of $[Ph_3PBn]_2[MnBr_4]$ in its glass state with a UV lamp. Despite the amorphous state, the salt was still able to emit green light. The reason behind this phenomenon could be related to the fact that the $[MnBr_4]^{2-}$ tetrahedra retain a rather rigid conformation, without allowing an excessive distortion of the geometry of the complex in the excited state or hindering in general the chances of non-radiative deactivation even in the amorphous glass state. This feature could be exploited for the formation of an emissive amorphous layer, often utilized in LEC fabrication.

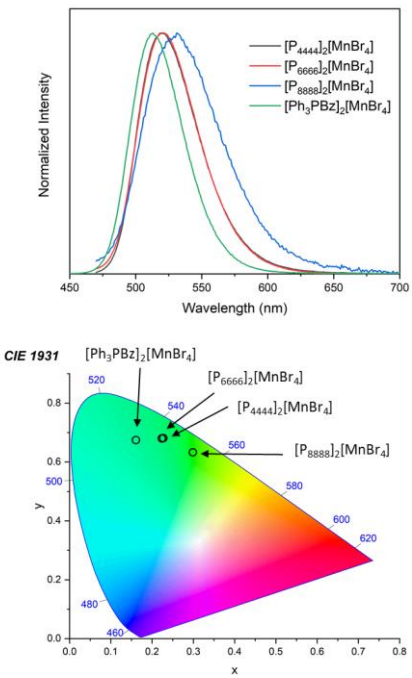

Figure 14. Photoluminescence spectra and relative CIE 1931 coordinates of $[P_{4444}]_2[MnBr_4]$, $[P_{6666}]_2[MnBr_4]$, $[P_{8888}]_2[MnBr_4]$, and $[Ph_3PBn]_2[MnBr_4]$.

All the ionic compounds revealed to be not only photoluminescent but also electroluminescent. Unfortunately, it was not possible to record the electroluminescent spectra of any of them due to the sensitivity of the instrument, but the observed emission still has important qualitative value, which let us speculate on their possible application in electrochemical devices. In all the cases, the luminescence seemed to not have dramatically shifted from the one recorded *via* photoexcitation. The observed electroluminescence is pictured in **Figure 15**, and it was induced by exciting vacuum-sealed Schlenk tubes containing the luminescent materials with an electric spark.

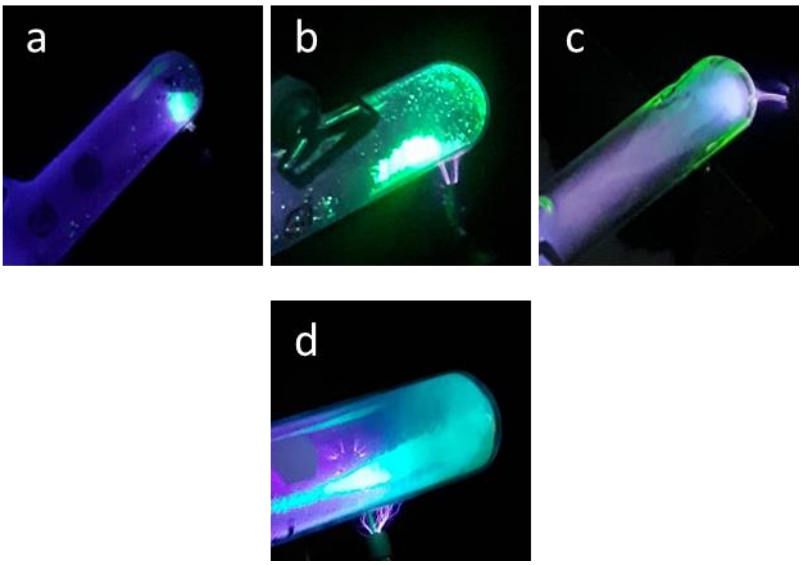

Figure 15. Electroluminescence of $[P_{4444}]_2[MnBr_4]$ (a), $[P_{6666}]_2[MnBr_4]$ (b), $[P_{8888}]_2[MnBr_4]$ (c), $[Ph_3PBn]_2[MnBr_4]$ (d).

3.3 Cyclic Voltammetry of luminescent Mn(II)-based ionic materials and white LEC based on $[Ph_3PBn]_2[MnBr_4]$

For application in electroluminescent devices, it is extremely important to estimate the energy of the HOMO and LUMO (or, more precisely, of the valence and conductive bands) of the materials. This helps to identify the supporting materials that compose the device, in order to have proper electron and hole transportation. To do so, cyclic voltammetry is one of the most suitable techniques. In a system like the one presented in section 2.2.1, the current flow

is recorded while changing the potential and it will increase intensity in correspondence to electrochemical processes. Scanning toward positive potential will reveal the oxidation processes while scanning toward negative potentials will spot the reduction processes. For the material herein investigated, the first oxidation process corresponds to the removal of one electron from the valence band (or HOMO), while the first reduction process indicates the injection of one electron into the conduction band (or LUMO).

Regarding the Mn(II)-containing salts, the oxidation process was always easily detected, while the reduction one exhibited low current intensity. In the case of the tetraalkyphosphonium, we used the data obtained from the absorption spectra to calculate *via* Tauc plot the energy of the LUMO. For the $[Ph_3PBn]_2[MnBr_4]$, it was possible to obtain satisfactory results with just the cyclic voltammetry data. Additionally, these results were also confirmed with the support of the absorption spectrum and the calculated Tauc plot. Overall, the electrochemical bandgap resulted to be wide, around 2.6 eV for all the tetrabromidomanganates.

Due to the high photoluminescence QY of $[Ph_3PBn]_2[MnBr_4]$, we decided to test how a LEC would perform when integrating into the active layer. For the device structure, we followed a host-guest approach. This method consists in mixing in the active layer charge-transporting material (host) together with a small percentage of emitting material (guest). LECs adapting this strategy have increasingly attracted the attention of researchers in the field because of their ability to overcome drawbacks characteristic of LECs built according to a more classic design.[134–137] In our case, we chose our host blend by taking inspiration from the OLED device built by L.-J. Xu and collaborators, in which the very similar $[Ph_4P]_2[MnBr_4]$ was used as the emitter.[89] The hole and electron transporting materials they employed were tris(4-carbazoyl-9-ylphenyl)amine (TCTA) and 2,6-bis(3-(9H-carbazol-9-yl)phenyl)pyridine (26DCzPPy), respectively. As the energy diagram presented in **Figure 16** is showing, the energy levels of these materials are compatible with the energy levels of our $[Ph_3PBn]_2[MnBr_4]$, making them suitable for the host matrix. The so chosen host materials and the guest $[Ph_3PBn]_2[MnBr_4]$ were mixed together and with the supporting IL tetrahexylammonium tetrafluoroborate ($THABF_4$), which was found to be necessary to increase the ion mobility and thus obtain detectable electroluminescence. The so prepared active layer was sandwiched between PEDOT:PSS on ITO-glass and vapor deposited Al (**Figure 16**). Two different LECs were prepared with different amounts of guest: 10% w/w (LEC1) and 20% w/w (LEC2).

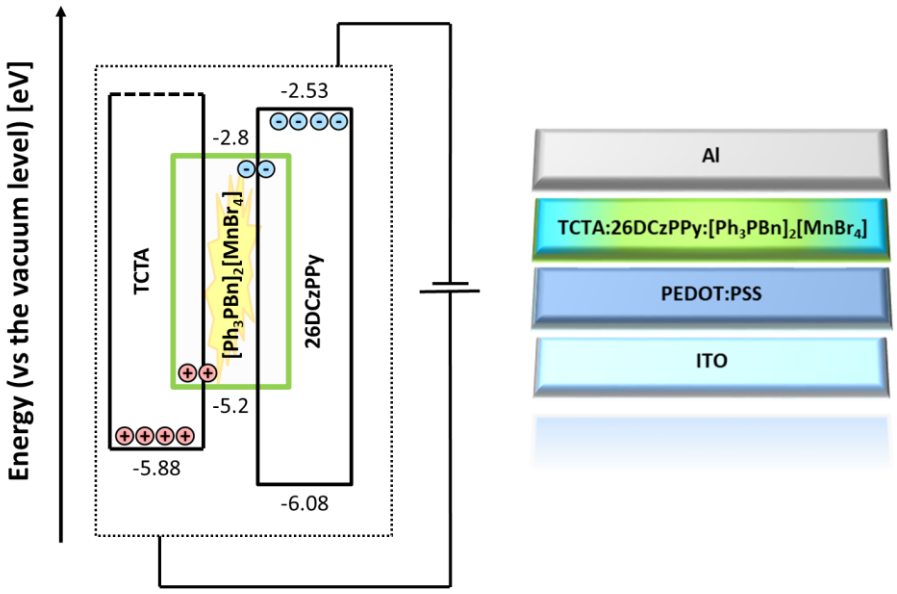

Figure 16. Energy diagram for the host and guest materials (*left*); LEC structure (*right*).

The devices surprisingly revealed white electroluminescence (EL) with a predominant peak in the red region of the visible spectrum (**Figure 17**). The reason behind this behavior was investigated with further analysis and led to the formulation of hypotheses, especially since none of the energy gaps observable in **Figure 16** corresponds to the energy of red light emission. We recorded the photoluminescence of the LECs in different moments of the lifetime, from prior to utilization, to post-mortem. The photoluminescence (PL) of the just prepared LECs revealed only the contribution of the blue emission of the host materials and the green emission of the guest, while the PL spectra collected after the cells were left running for about two minutes exhibited the band in the red region of the spectrum. Additionally, the green emission of the $[Ph_3PBn]_2[MnBr_4]$ showed to decrease in intensity across the lifetime of the LECs. This made us formulate the hypothesis that while the LECs are operating, the $[MnBr_4]^{2-}$ tetrahedra could drift under the action of the applied bias and therefore come in contact with each other to form octahedral or trigonal bipyramidal complexes (**Figure 18**). This is in line with the progressive formation of red-emitting Mn(II) complexes and the consequent loss of green-emitting ones, rather than exciplet emission due to the interaction with the host materials. In fact, the exciplet emission should appear right after the host-guest layer formation, but this was not observed in our case. Moreover, a behavior similar to the one we described has been reported in the study by Y. Rodríguez-Lazcano and collaborators,[138] where $[MnX_4]^{2-}$ tetrahedra (X = Cl or Br) converted into red-emitting species under stress in form of pressure,

and in the previously mentioned study by Z. Huang and collaborators, where the transition of ILs to LC phases led to the formation of $[MnCl_2Br]^-$ red-emitting species.[88]

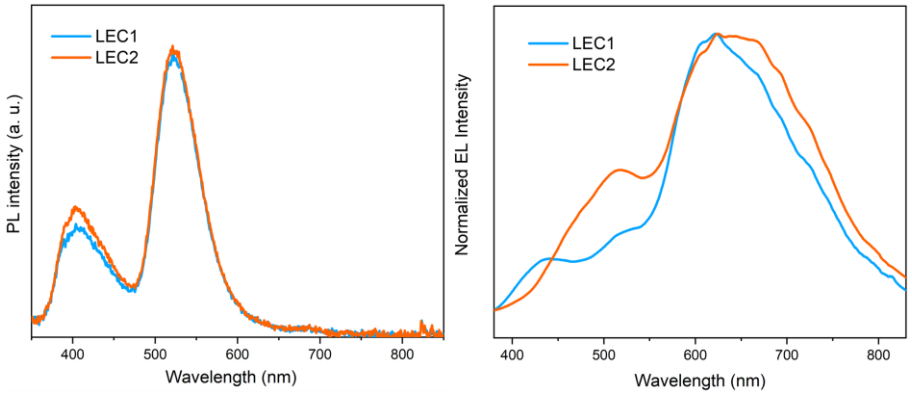

Figure 17. Photoluminescence (*left*) and electroluminescence (*right*) spectra of the prepared LECs.

Overall, our findings show how the asymmetric $[Ph_3PBn]_2[MnBr_4]$ was successfully employed as a practical dual emitter for monocomponent white LECs. The adopted design allowed the *in situ* formation of red-emitting species that additionally gave a major contribution to the LEC spectra. Most likely, this is the result of the highly mobile environment surrounding the $[MnX_4]^{2-}$ tetrahedra, which was provided by the asymmetric cations and the supporting IL.

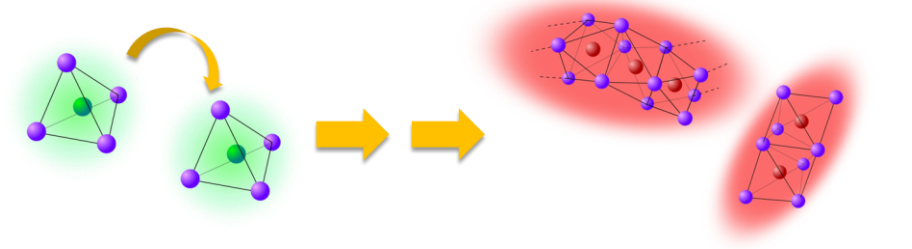

Figure 18. Proposed mechanisms for the formation of red-emitting Mn^{2+} octahedra.

4. Paper III: Fully organic small molecules as emitters

4.1 8-Hydroxyquinolines IL-like thermal properties

In Paper III, we attempted to synthesize IL-SM by combining the luminescent $[8HqH]^+$ cation with the bis(trifluoromethanesulfonyl)imide $[Tf_2N]^-$, which is extensively used for the synthesis of ILs due to its flexibility and chemical stability.[139–142] We expanded our research by functionalizing the cation with one methyl group in position 2 (on the pyridinic ring) $[2Me8HqH]^+$ and position 5 (on the phenolic ring) $[5Me8HqH]^+$. The methyl group has an electron-donating nature and the introduction of this group in different positions was expected to affect the electron cloud and therefore to perturbate the energy levels of the molecule. This allowed us to better explore and understand the photophysical properties of these compounds.

The DSC curves of the synthesized salts (**Figure 19**) demonstrated a typical profile for ILs, but $[8HqH][Tf_2N]$ and $[2Me8HqH][Tf_2N]$ presented a temperature of melting higher than 100 °C, therefore formally violating the definition of ILs. While $[8HqH][Tf_2N]$ and $[2Me8HqH][Tf_2N]$ melted, respectively, at 113 °C and 130 °C, $[5Me8HqH][Tf_2N]$ melted at 99 °C. Additionally, the first two compounds were both characterized by a strong supercooling ($\Delta T_{supercooling}$) of 46 °C and 40 °C, respectively, while $[5Me8HqH][Tf_2N]$ showed a much smaller $\Delta T_{supercooling}$ of 17 °C. This is the result of a crystallization hindering, which is a common feature for ILs.[3] This behavior could be exploited in the field of electroluminescent device fabrication, allowing solvent-free layer formation through the application of supercooled materials.

SCXRD was performed for all three compounds, revealing an intricate network of hydrogen bonds and π-stacking (**Figure 20**). The latter always involved the stacking of one moiety of the cation (phenolic or pyridinic) and a different one from a neighboring cation. In the structure of [8HqH][Tf_2N] and [5Me8HqH][Tf_2N], this resulted in the formation of continuous columns of cations in what we called a stair configuration, while the cations of [2Me8HqH][Tf_2N] organized in dimers. Both hydrogen-bond and π-stacking interactions are the reason why the compounds exhibit a high tendency to crystallize, besides the "quenching" presence of the [Tf_2N]$^-$.

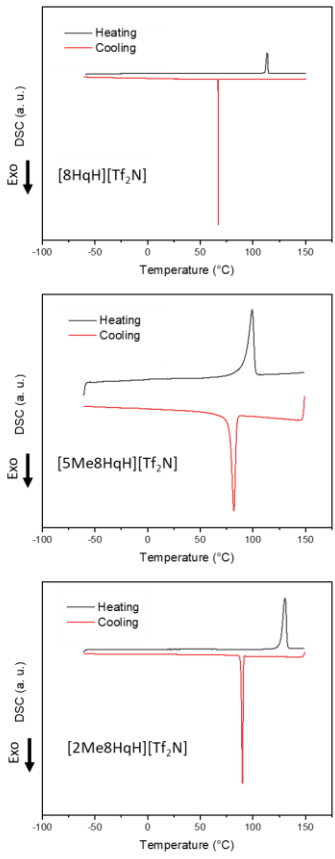

Figure 19. DSC curves of the obtained 8-hydroxyquinolinium salts.

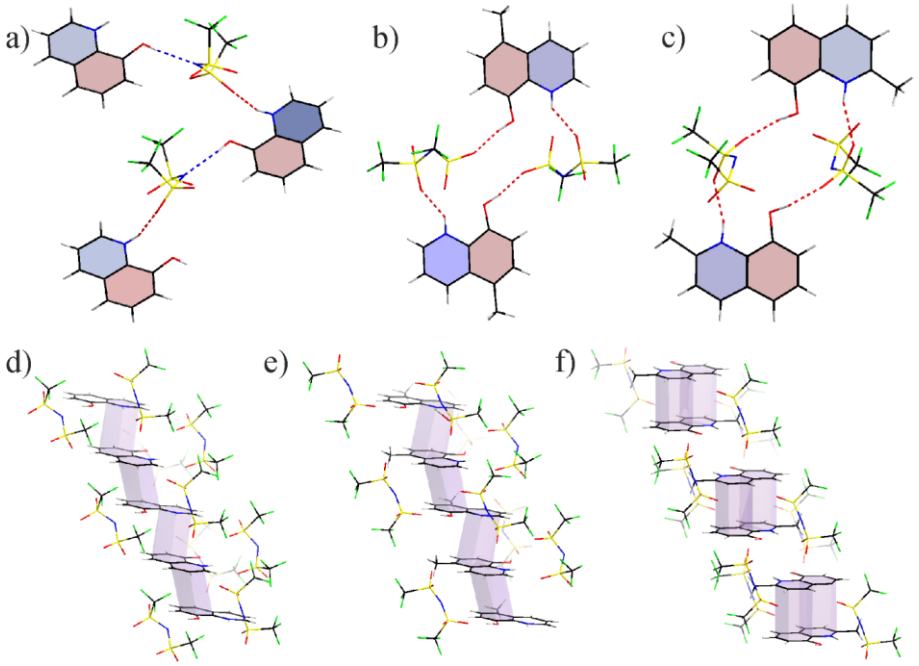

Figure 20. Representation of the strongest hydrogen bond connectivities in [8HqH][Tf_2N] (a), [5Me8HqH][Tf_2N] (b), and [2Me8HqH][Tf_2N] (c) together with the respective stair ([8HqH][Tf_2N] (d) and [5Me8HqH][Tf_2N] (e)) and dimeric ([2Me8HqH][Tf_2N] (f)) π–π stacking forming the crystallographic networks.

4.2 The effect of methyl-substitution on the luminescence of $[8HqH]^+$ salts

Differently from the just discussed materials, the $[8HqH]^+$ salts presented in Paper III do not rely on a metal center for light emission, but rather on the fluorescent quenching of the excited states of the cations.

All the $[8HqH]^+$-based ionic compounds revealed blue or green-blue emission under UV photoexcitation (**Figure 21**) and their properties were investigated in solid-state, in aqueous solutions (2.0×10^{-4} M), and in the supercooled state to unravel more details of their luminescence properties. DFT calculations were performed to have a deeper understanding of the luminescent mechanism and nature. From the results of DFT calculations, the HOMO and LUMO of 8Hqs-based compounds were located on the phenolic and pyridinic rings, respectively (**Figure 22**). Since the addition of a methyl group in position 2 or 5 affects the energy of the molecular orbitals due to its electron-

donating nature (as also confirmed by DFT), the luminescence of the compounds is also affected. More specifically, the methyl group increases the energy of the molecular orbitals located on the functionalized ring. Therefore, we expected a narrowing of the HOMO-LUMO gap for [5Me8HqH][Tf_2N] (an increase of the energy of the HOMO) and a widening for [2Me8HqH][Tf_2N] (an increase of the energy of the LUMO) when compared with the unsubstituted [8HqH][Tf_2N]. This would lead respectively to a redshifted (less energetic) and a blue-shifted (more energetic) emission.

The emission of solid [8HqH][Tf_2N] (λ_{ex} = 400 nm) was represented as a broad curve with a maximum at 460 nm, originating from π^*-π transitions of the $[8HqH]^+$ unit. The methylated relatives followed the expected trend. Solid [5Me8HqH][Tf_2N] was characterized by a redshifted emission with the emission peak at 488 nm (λ_{ex} = 420 nm), while the one of [2Me8HqH][Tf_2N] was slightly blueshifted with the peak at 393 nm (λ_{ex} = 400 nm). The color difference is more clearly displayed with a CIE 1931 diagram (**Figure 21**). The obtained QYs and lifetimes of each compound were, respectively, 20% and 40 ns for [8HqH][Tf_2N], 13% and 24 ns for [5Me8HqH][Tf_2N], and 49% and 47 ns for [2Me8HqH][Tf_2N], with all the lifetimes fitting a monoexponential decay. These photophysical properties are comparable with the ones reported for other metal-hydroxyquinoline-based materials, which have found application in OLEDs.[143–148]

The investigation of the luminescence in solutions and supercooled states revealed the role of the rigid network built between the ions in the crystalline state. When the herein-presented salts were dissolved in water, the broad band emissions resulted blue-shifted because of the solvatochromic effect of the polar solvent. Additionally, the intensities were not strong enough to allow QY or lifetime determination. Most likely, the cations (the only ions responsible for the light emission) were not locked anymore in place *via* hydrogen bonds and π-stacking, but rather surrounded by polar molecules. In these conditions, the excited states could deactivate through the fast proton transfer mechanism previously discussed,[104] leading to fluorescence quenching and therefore to the negligible luminescence of the solutions.

For the measurements in the supercooled state, the compounds were heated above the melting point and then cooled down to lower temperatures, but still higher than the crystallization point. Also in this case, the luminescence of the compounds was quenched. The extremely weak fluorescence obtained after photoexcitation was redshifted for all the compounds and it was not possible to record QYs and lifetimes as well as for the aqueous solutions. The redshift and the quenching were explained as the result of increased vibrational freedom of the cations in a liquid-similar state that is the supercooled state, which

led to the formation of aggregates and motion-related non-radiative deactivation mechanism.

As for the Mn(II)-based emitters, the electroluminescence of these SMs was investigated. Also for these materials, the electroluminescence allowed only for qualitative analysis (**Figure 23**), revealing their blue emission, which intensity trend resembled the photoluminescence ones ([5Me8HqH][Tf_2N] < [8HqH][Tf_2N] < [2Me8HqH][Tf_2N]).

As for the Mn-based emitters, analysis with cyclic voltammetry was performed also on 8HqH-based materials. The obtained curves exhibited clear quasi-reversible processes in both reduction and oxidation. The bandgaps followed the trend identified with DFT calculations and were reproducible over multiple cycles.

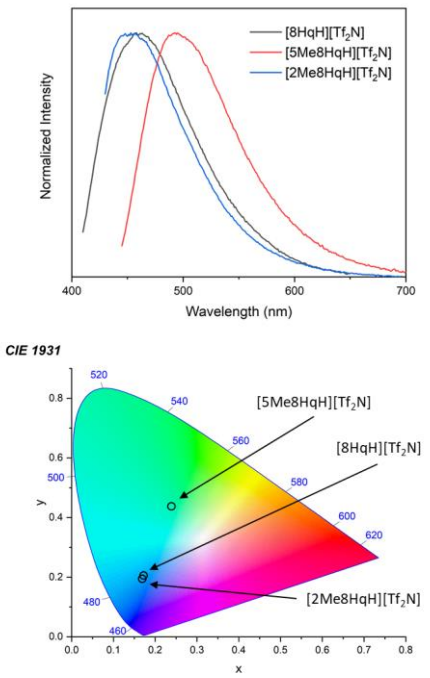

Figure 21. Photoluminescence spectra and relative CIE 1931 coordinates of [8HqH][Tf_2N], [5Me8HqH][Tf_2N], and [2Me8HqH][Tf_2N].

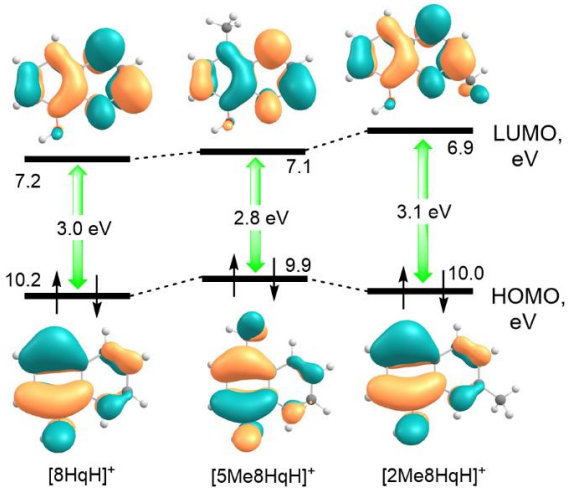

Figure 22. The shape and energy of frontier molecular orbitals for $[8HqH]^+$, $[5Me8HqH]^+$, and $[2Me8HqH]^+$ species.

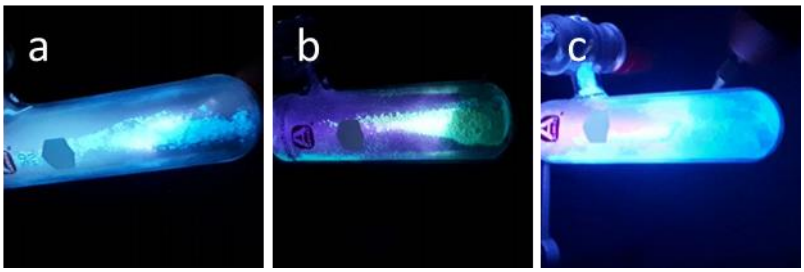

Figure 23. Electroluminescence of $[8HqH][Tf_2N]$ (a), $[5Me8HqH][Tf_2N]$ (b), and $[2Me8HqH][Tf_2N]$ (c).

5. Paper IV: ILs with photoswitchable properties

5.1 Azobenzene photoisomerization

ILs can be easily functionalized through substitution reaction, and recent examples of azobenzene-ILs (azo-ILs) have been demonstrated to be an optimal scaffold for various applications. Appropriate functionalization of azo-ILs has led to light-controlled ion transporters[149] and time enhancers for drug delivery systems.[150] Some ILs can exhibit LC mesophases and this is also the case for azo-ILs.[151] Such compounds have been studied, showing the effect of the ionic character on mesomorphic behavior,[152] developing ILs with photochromic functionalities[153] or photoresponsive conductivity.[154]

Having this kind of background, we have found interest in synthesizing a series of azo-ILs bearing different substituents on the azobenzene moiety and investigating their effect on *cis-trans* conversion efficiency and thermal behavior. For this purpose, the ILs studied for Paper IV and presented in this chapter were sharing the chemical structure presented in **Figure 24**. The azobenzene group was connected to a dodecyl-imidazole group through an ether link. In this way, the cationic moiety would act as a mesogenic group, while more flexibility was assured by the connecting bridge. Different substituent groups -R were located on the opposite end of the photoswitchable azobenzene unit, in the *para* position. To properly investigate the effect of this group, a wide array of functions were taken into consideration, such as methyl- (Me, (**1**)), *tert*-butyl- (*t*-Bu (**2**)), methoxy- (OMe (**3**)), *N*,*N*-dimethylamino (NMe_2 (**4**)), and nitro (NO_2 (**5**)) groups.

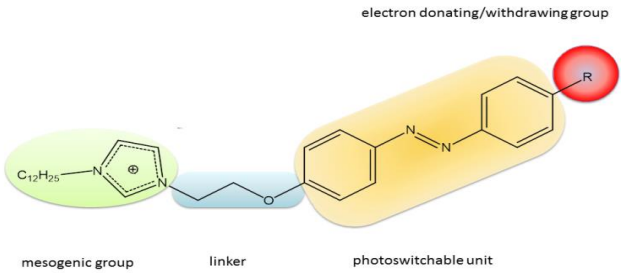

Figure 24. The general structure of the studied compounds (R = Me (**1**), *t*-Bu (**2**), OMe (**3**), NMe_2 (**4**), and NO_2 (**5**) (Adapted with permission from Paper IV).

5.2 The effects of substituents on thermal properties

Thermal analyses through DSC revealed the phase transitions that characterize the obtained compounds. Only compounds **2** and **4** showed a melting temperature below 100 °C (99.5 °C and 63.6 °C, respectively) fulfilling the requirement for being defined as ILs. Nevertheless, all the compounds showed thermal properties characteristic of ILs, such as supercooling (the recrystallization from the melt at a temperature significantly below the melting point), crystallization during the heating process, or a mesophase (**Figure 25**). The latter has been identified for **1**-**4**, but not for **5**, which reveals only a direct phase transition from solid to isotropic liquid. All the others, instead, presented a SmA LC phase, which was identified by POM. Azo-compound **1**, **2**, and **4** showed the transition while heating, the SmA LC phase was revealed by an oily streak texture. Instead, **3** showed focal conic texture upon cooling as the distinctive indication of a SmA phase (**Figure 26**).

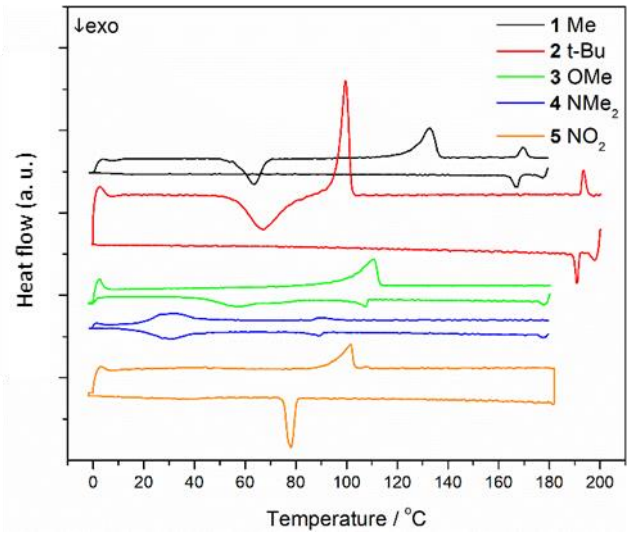

Figure 25. DSC thermograms of compounds **1-5**. For each compound, the upper line corresponds to the 2nd heating curve, while the lower line corresponds to the 2nd cooling (Adapted with permission from Paper IV).

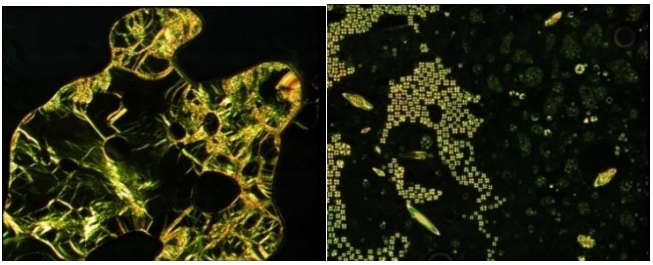

Figure 26. Representative textures as seen between crossed polarizers: (*left*) oily streak texture of compound **2** at 103.1 °C, (*right*) focal conic texture upon cooling of compound **3** at 107.3 °C (Adapted with permission from Paper IV).

Even though crystals suitable for X-ray diffraction analysis were successfully grown only for **1-3**, it was still possible to get an insight into the structural effect of the -R group, which then affected the thermal properties. The methoxy group of **3** most likely stabilized the crystal formation and hindered the mesophase formation through a CH---O electrostatic hydrogen bond (2.89 Å) with a neighboring azobenzene ring. This could not occur with **1** or **2**, since their substituents were alkyl groups, without an electronegative heteroatom. Additionally, compounds **1-3** showed that the azo-cation bent to form a "U" shape, having the R group of a unit facing the neighboring one (*e. g.* **1** in **Figure 27**). In this way, it was possible to explain why **4** presented the smallest mesophase temperature window of 58.4 °C (in contrast to the wide 100 °C of

2) and why **5** did not form an LC phase. Since both compounds have a polar group (NMe_2 (**4**) and NO_2 (**5**)), close contacts between them would result in repulsive forces, hampering the recrystallization. For **1**-**3**, instead, *van der Waals* forces between the –R groups would pull the different molecules together, forming crystalline and LC phases.

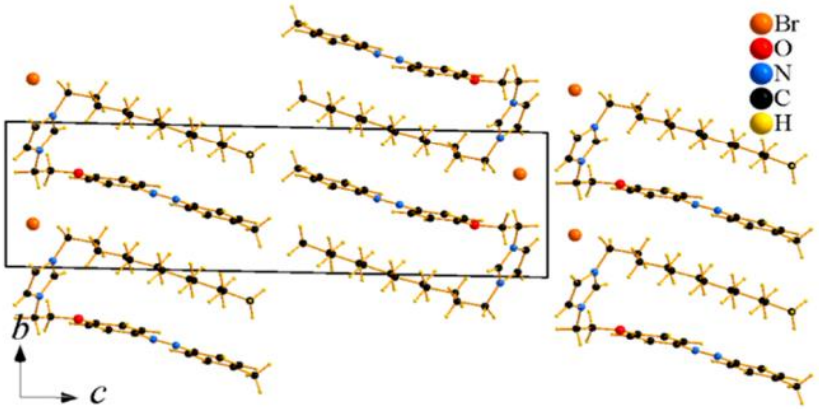

Figure 27 Projections of the crystal structure of compound **1** on the *bc* plane showing the "U" shape formed by the azo-cations (Adapted with permission from Paper IV).

5.3 The effects of substituents on photochromic properties

The photochromic properties of each azo-IL were investigated through UV-Vis absorbance measurements. Methanolic solutions of the compounds revealed a common profile, with a peak between 340 nm and 410 nm and one less intense at lower energies, between 430 nm and 440 nm (**Figure 28**). Time-dependent density functional theory (TDFT) calculations and bibliographic research made it possible to define the transitions responsible for the identified absorption bands as π-π* (340-410 nm) and n-π* (430-440 nm) of the *trans* isomer.[155,156] While the energy of the n-π* band barely variated between the different compounds, the π-π* band was revealed to be shifted. All the shifts of the π-π* band seemed to be related to the electron-donating ability of each –R group. In fact, the π-π* band progressively redshifted following the order: Me (**1**) < *t*-Bu (**2**) < OMe (**3**) < NMe_2 (**4**). Contrarily to this trend, the compound with NO_2 (**5**) revealed the highest red-shift, besides its low electron-donating strength.

Upon UV irradiation, the intensity of the π-π* band decreased and blue-shifted, while the n-π* one increased in intensity as an effect of the photoisomerization to *cis* conformation. In the *cis* form, the π-conjugation of the azobenzene group diminished, increasing the HOMO-LUMO energy gap and thus causing the blue shift. This does not occur for **4** nor for the other azo-ILs because the π-π* and the n-π* overlap, indicating extremely close energy levels for the two isomers and therefore a fast relaxation from *cis* to *trans*. Therefore, it was possible to define the efficiency of photoconversion by relying on the magnitude of the blue-shift. This revealed that **3** has the highest efficiency of photoisomerization to *cis* of 92% (blue-shift of 42 nm) among the set of compounds, immediately followed by **2** with 90% (blue-shift of 40 nm).

Ultimately, the substitution in the *para* position of the azobenzene group leads to strong differences in the thermal and photochromic behavior of the synthesized azo-ILs. This revealed how a watchful choice of electron-donating or electron-withdrawing substituents could allow the achievement of specific structural interaction for *ad-hoc* photoresponsive ILCs. Similar materials could find applications as sensors and in related fields.

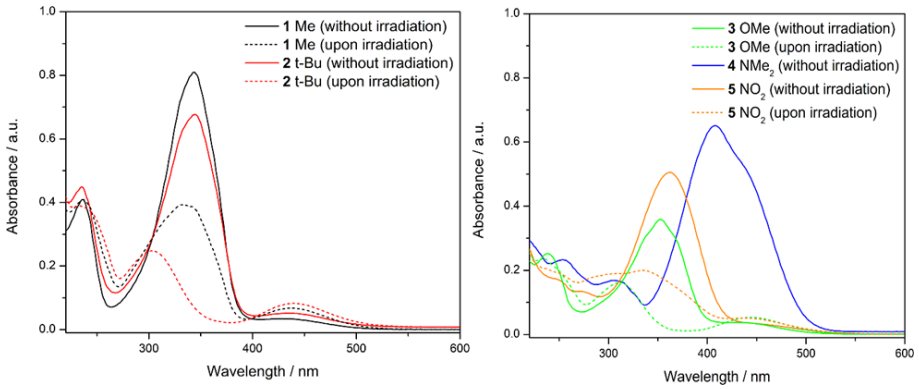

Figure 28. Absorption spectra of methanolic solution of **1-5** before (*solid lines*) and after (*dotted lines*) UV irradiation. (Adapted with permission from Paper IV)

6. Paper V: Triazolium ILs for application in DSSCs

6.1 Triazolium ILs with LC phases

While imidazolium-based ILs are one of the most diverse and studied classes of ILs and, as was discussed above, some of them have shown the ability to organize in an LC phase,[157,158] it has been proven that ILs having a triazolium as a cationic moiety show more stable mesophases.[159–161] This can be linked to the ability of the molecule to form hydrogen bonds. The presence of an N atom in position 2 instead of the C-H fragment should lead to a wider temperature stability range for the LC phase. Additionally, the most common decomposition process for imidazolium ILs is through radical carbon formation in position 2, which is therefore completely avoided in triazolium ILs. In the study presented in Paper V, we compared asymmetric 1-alkyl-3-methyltriazolium ILs, symmetric 1,3-alkyl-1,2,3-triazolium, and already reported asymmetric 1-alkyl-3-methylimidazolium iodides to prove their positive effect on the performances of the DSSCs (**Figure 29**).

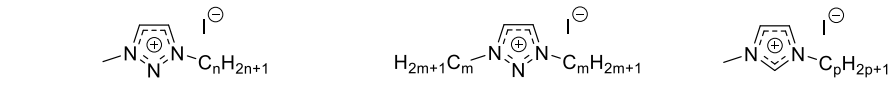

Figure 29. Representation of the studied ILs: asymmetric (*left*) and symmetric (*middle*) 1,3-dialkyl-triazolium iodides. Related 1-alkyl-3-methylimidazolium iodides (*right*) were studied for referencing as we use a different experimental setup compared to the literature (Adapted with permission from Paper V).

Despite our design intent, not all the synthesized triazolium salts have shown a transition to a mesophase before melting. POM analyses of 1-dodecyl-3-methyltriazolium iodide (**1**) and 1-undecyl-3-methyltriazolium iodide (**2**) allowed the observation of their mesophases which presented an oily streak texture under POM and were therefore recognized as SmA. Instead, the symmet-

ric 1,3-didecyltriazolium iodide (**7**) and 1,3-dioctyltriazolium iodide (**8**) exhibited SmC phases, recognizable from their marble Schlieren texture (**Figure 30**). Noteworthy, all the other compounds revealed a melting temperature below 100°C, therefore being classified as ILs.

As it has previously mentioned, DSSCs require a redox couple to work properly. Therefore, 25 mol% of I_2 was added to each IL to generate the I^-/I_3^- couple. As a consequence, the thermal behavior of each IL changed, revealing a decrease in the melting point. This was also followed by the widening of the LC mesophase window of the ILs that were presenting it. This addition affected also the conductivity of the materials, but this matter will be discussed in the following subchapter.

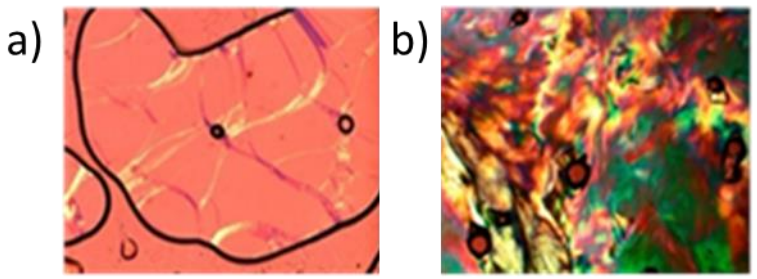

Figure 30. Representative textures observed between crossed polarizers under an optical microscope. a) SmA phase of **1** at 97.4 °C and b) SmC phase of **8** at 58.2 °C (Adapted with permission from Paper V).

6.2 Conductivity and DSSCs performances

To apply the triazolium ILs in an electrochemical device such as the DSSCs, it was important to assess their conductivity. This was done while tuning and monitoring the temperature and, as expected, the conductivity increased with the temperature because of the increased mobility of the ions. The same temperature-dependent conductivity measurements were performed after the addition of 25 mol% of I_2, revealing more interesting results. The conductivity at operating temperature (40 °C) escalated dramatically, generally going from less than 1 μScm^{-1} to more than 800 μScm^{-1} (**Figure 31**). Additionally, cyclic voltammetry analyses demonstrated wide electrochemical stability, characteristic for ILs, without showing signs of electrode passivation by the I_2, which is normally encountered with imidazolium iodide ILs. This gave high hopes for their performances in devices.

DSSCs were therefore prepared with these 1,3-dialkyltriazolium triiodide ILs and their performances were tested. When compared with DSSCs having imidazolium ILs, our cells demonstrated not only higher efficiency but also higher stability over time (**Figure 31**). While the triazolium-DSSCs did not show a significant efficiency loss over two months, the imidazolium ones had a 5-10% efficiency loss. This can be related to the stability of the triazolium ILs and their non-hygroscopicity, while DSSCs with imidazolium ILs were more likely affected by the capture of moisture.

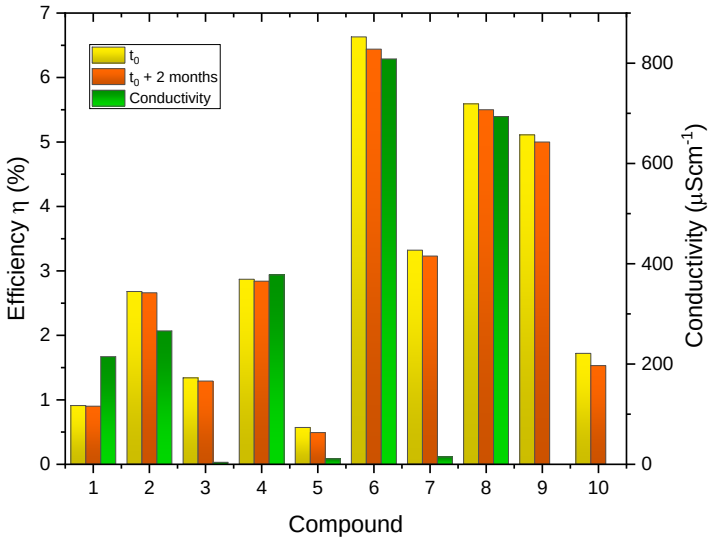

Figure 31. Efficiencies of the investigated DSSCs at t_0 and t_0 + 2 months together with the conductivity of 1,3-dialkyltriazolium iodide ILs with 25% mol I_2 at the working temperature of 40°C.

In conclusion, the synthesized triazolium iodide and triiodide ILs demonstrated greater potential than their imidazolium counterparts in terms of stability and performance, also showing wide and stable LC mesophases. When utilized inside DSSCs, the triazolium ILs showed better results than the ones made with imidazolium, showing less decay over time. These compounds demonstrate how the triazolium ILs and salts have design-related properties that provide these materials with a high potential for application as electrolytes in efficient and stable DSSCs.

7. Concluding Remarks

ILs are an extremely versatile class of materials that allows diving into the fourth state of matter, the mesophases. Exploration of their properties through thermal (DSC), optical (POM), and diffraction techniques (SCXRD, PXRD) permits the understanding of the interactions underlying their behavior. Thus, the obtained information provides tools for the design of ionic materials with specific physicochemical features.

Materials combining ionic conductivity and low melting point with an almost absent vapor pressure could revolutionize (and are revolutionizing) the field of electrochemical devices. This thesis work presents a wide collection of ionic compounds that were prepared and characterized foreseeing their application in such systems, mainly focusing on light-emitting or light-absorbing devices. Four classes of widely studied P-based (phosphonium) and N-based (imidazolium, triazolium, 8-hydroxyquinolinium) cations have been utilized for the synthesis of the final materials, while halides, $[Tf_2N]^-$, and $[MnBr_4]^{2-}$ were adopted as anions.

The four phosphonium-based materials bearing the $[MnBr_4]^{2-}$ emitting centers have demonstrated peculiar thermal properties together with green photo- and electroluminescence. While $[P_{4444}]_2[MnBr_4]$ and $[P_{8888}]_2[MnBr_4]$, the materials with the respectively shortest and longest organic groups, were ILs, the "intermediate" materials $[P_{6666}]_2[MnBr_4]$ and $[Ph_3PBn]_2[MnBr_4]$ revealed melting point above 200 °C. The $[P_{6666}]_2[MnBr_4]$ showed phase transitions whose entropies hint at a plastic crystal nature, making this material the first with these rather large ions. Unfortunately, a precise definition of the structure was not possible, leaving a shade of uncertainty. The highly emissive $[Ph_3PBn]_2[MnBr_4]$ was successfully adopted in white LECs, exhibiting a double green-red emission achieved *via* drifting of the ions towards the electrodes, which most likely caused the formation of different coordination of the Mn(II) metal center.

Three salts based on 8-hydroxyquinolinium and $[Tf_2N]^-$ pushed the arbitrary boundaries of ILs, exhibiting supercooling but melting slightly above the

100 °C threshold. Intricate crystal structures relying on π-stacking and hydrogen bonds reveal to be the reason for the efficient blue luminescence rising from the cations and most likely the “high” melting point.

The imidazolium ILs were functionalized with azo-benzene photoswitchable units having different functional groups in *para*. These functions affected strongly the ability of the ILs to form mesophases due to the interactions between the ionic moieties while retaining the ability to switch between *cis* and *trans* isomers. The reversibility of the process was still bonded to the nature of the group in position *para* and it has been determined *via* evaluation of the π-π* UV-Vis absorption band.

Finally, the mesophase formation of triazolium ILs has been analyzed in relationship with the length of the alkyl chains bonded in positions 1 and 3. We found that only the ILs with chains exceeding a threshold of eight carbons were able to form mesophases. Expected to have more stability than the imidazolium relatives due to the absence of the carbon atom in position 2, these ILs have been applied in DSSCs as intermediate electrolytes, proving their higher performances. Additionally, cyclic voltammetry investigations did not reveal the passivation of the electrodes by the I^-/I_3^- couple, a common drawback of this redox mediator.

8. Outlook

The collection of ionic materials explored in this work has demonstrated properties that are of utmost importance for the advancement of photoelectrochemical devices. The "ionic liquid approach" that has been taken for the design of such compounds aims to give the basis for innovative solutions for the advancement of the field. Additionally, the pairing of structural and thermal properties gives great insight into the ability of these materials to form mesophases or exhibit supercooling, therefore helping future research for the tailoring of *ad hoc* ionic materials.

The series of Mn(II)-based materials spaces across the whole range of states of non-gaseous materials, going from the RTIL $[P_{8888}]_2[MnBr_4]$, to the IL $[P_{4444}]_2[MnBr_4]$ exhibiting a SmA mesophase, to the (most likely) plastic crystal $[P_{6666}]_2[MnBr_4]$, to the crystalline $[Ph_3PBn]_2[MnBr_4]$. The application of the latter in host-guest LECs has opened a door toward single-emitter broadband white LECs. More research aimed at the improvement of the performances of this kind of device will allow the fabrication of more efficient and low-cost apparati. Moreover, the $[P_{4444}]_2[MnBr_4]$ could find application in devices where the layer formation is not bounded to the need for a solvent, while the mesophases of $[P_{6666}]_2[MnBr_4]$ could well be further explored for application in solvent-free devices.

The 8HqH-based SMs are the first example of extremely small and easily synthesizable blue-light emitters. Their supercooling and low melting temperature could be adopted for solvent-free processing for application in light-emitting devices, even if more research will be needed to overcome their high crystallinity and obtain the adequate amorphous substrate (e.g. embedding in a host material, control of spin-coating parameters).

The investigations on the azo-imidazolium ILs and triazolium ILs and the effect of substituent groups on the mesophase formation could lead to their application in photoresponsive devices and innovative more stable DSSCs, respectively. Moreover, the obtained results could be used as a starting point for even more stable ionic materials that could even see their utilization by the wide public.

9. Acknowledgements

First, I have to thank my supervisor Prof. Dr. Anja-Verena Mudring for the opportunity to conduct my PhD with her. After a life spent in my hometown in Italy, you gave me the chance to widen my intellectual reach, granting me to explore the world of international academic research. Needless to say that this made me grow as a scientist also thanks to the many colleagues I worked with and the techniques I have learned. At the same time, these years made me grow also as a person, allowing me come out of my shell and ready to take on new challenges. Thank you for this invaluable chance.

I would like to thank my co-supervisor Prof. Dr. Lars Kloo for the support received during these years. You always had supporting and wise advices even when I was hitting a rough patch. Thank you for the help towards the way of professional behavior.

I would like to thank Prof. Dr. Robin D. Rogers and Prof. Dr. Ludvig Edman for the collaboration and the scientific guidance.

I want to thank Dr. Guillaume Bousrez for his help. We started builing the laboratory together and from the mounting of the support for the Schlenk lines until the end of my PhD you were beside me all the time. I learned so much about working in a lab due to you. Now I know that I have two hands and I can even use them at the same time! Thank you for all the discussions in and out the lab and your extreme support during the last years.

I would like to thank Dr. Volodymyr Smetana for the discussions we had, the help on the crystallographic part of my PhD, and the support on the manuscripts.

A special thanks goes to Dr. Safak Bulut, Dr. Chris R. Celania, Dr. Katahrina Dorn, Dr. Oliver Hammond, Dr. Alexander Ovchinnikov, Dr. Veronica Paterlini, Dr. Sebastien Preaud, Dr. Rui Shi, and Dr. Manish Shimpi. Interacting with you on the daily basis was amazing, a group of people that I know gave a lot to support me in my work and in my mental health. Our long discussions on science and life plus meeting outside the office are going to

always have a place in my heart and I am sure you will brighten up all the other colleagues you will meet in your carrer, as you did with me.

At the same time, the quality of my life in and outside the PhD would have been dramatically worse without many other people. First of all I want to thank Anthony Boudier, Dr. Olivier Renier, and Dr. Stefanie Siebeneichler. You have been extremely good friends, alaways by my side during both happy and (most importantly) bad moments. We laughed, we played, and we discussed a lot and those are moments that I cherish. I really hope that our roads will cross again. Dr. Thomas and Shiba (first of the two cats receiving acknowledgement), you, together with Steffi, were always there to support me, especially during the last years. You kept draggingme out of my place, always trying to keep me active and to spend time with you. I loved being "neighbours"and you felt like a family to me.

Another big family that keeps growing and growing and that I can proudly say to be part of is the one composed by the amazing Dodgeball Sweden and the Stockhol Dodgeball Associaton. Starting from the living legend Konstantin Kriechbaum, who convinced me to try this sport in the winter of 2019, this family gave me so much support, happy moments and friendship that I struggle to describe. For this reason, I want to thank Henric Carlsson, Pierre Corvellec, Felicia Strålin Edvardsen, Linda Eriksson, William Jewkes, Robert "Bob" Sundberg Johansson, Agnes Karlsson, Erik Liling, Gustav Liling, Ben Wolfgang McAdam, Linnea Widås Nero, Joel Palmert, Jacob Poyser, Faisal Raad, Nathaly Ruck, Twan Schreurs, Hanna Sonebäck, Marcus "Strumpa" Ström, Oscar Svernlov, Adnan Khan Wazir, and many others which I am not naming just for conciseness sake. I hope to stay in contact with you all and to meet again, maybe during a tournament!

I want to thank the gang that originated from the Organic Chemistry Department, which tried to involve me in multiple occasion for trips and activities during my stay in Stockholm. Thank you Matteo Costantini, Marie Deliaval, Davide Di Francesco, Ester Di Tommaso, Axel Furevi, Luca Massaro, Francesco Nosenzo, Alessandro Ruda, Federico Riu, and Emanuele Silvi for giving me a corner of Italy that made me feel less far from the homecountry. I hope to meet you again, even if scattered around the globe.

Italian support did not come only from the Arrhenius Laboratory. Thank you Anna Finozzi and Andrea Roda. Experts in fields different from mine and friends that I know I can trust. Thank you for the time spent together, the dinners and long discussion. I wish you good luck and I hope our streets will meet again.

Thank you Puma, my little creature of the darkness and second cat to be in this section. Even if you will never be able read these words, thank you for your purring, your head-butts and your weird meowing. You alleviated my soul every time you visited me.

I want to thank the group of people that I spent most of my evening at home with, between playing videogames, discussing about both light and heavy subjects, and even fighting. First of all, thank you Letiza Fratta (Ladytatian) and Marco Patronici (PatroGW), cornerstones of this group. I can't imagine what it would have been without you two. I want to thank also Steven Benedetti (Yohoku), Alessandro Ilias Azzaro (Prendiamoci), Andrea Di Maio (KuronoMayo), Michelangelo Frisoni (Alpha Chino), Daniele Frisoni (il fenicio), Claudio Popa (Lordherriork), Luca Roncone (luc4street), and Alessandro Swaab (Ruelfighter) for the time spent together even if we were thousands km apart.

I want to give a big thank to the friends that waited every summer and winter break to see me again, that were always ready to support me, help me or just have a talk on the phone. First of all, thank you Antonio "Tonno" Bianchi and Thomas Bigoni, I know you will always have my back and will always be there for me. Also thank you Giulia Borin, Luca Casini, Fulvio Gandini, Rossella Natalini, Alessandra Penoni, Simone Pini, Valentina Roncagli, Ilenia Settembrini, Michele Tortora, Stefano Tortora, Matteo Vagnoni, and Elena Venturoli. I am very happy to know you and for our bond. I wish that our friendship will last beyond our paths, now that we are well into the adulthood.

Finally, I want to thank my family. Mamma, Papà e Dafne, grazie per il vostro continuo supporto. Grazie per l'amore che continuate a dimostrarmi. Se sono arrivato dove sono oggi è anche merito vostro. Grazie a zia Antonella, zio Fabio, zia Michela, zio Raul, Andrea, Matteo, Niccolò e Petra, grazie per farmi sentire il vostro affetto in ogni occasione, anche se i nostri incontri sono stati sporadici negli ultimi anni. Grazie per essere la mia Famiglia.

10. References

[1] S. Gabriel, J. Weiner, *Berichte Dtsch. Chem. Ges.* **1888**, *21*, 2669.
[2] P. I. Walden, *Известия Российской Академии Наук Серия Математическая* **1914**, *8*, 405.
[3] A.-V. Mudring, *Aust. J. Chem.* **2010**, *63*, 544.
[4] P. Wasserscheid, T. Welton, *Ionic Liquids in Synthesis*, Wiley Online Library, **2008**.
[5] T. Welton, *Chem. Rev.* **1999**, *99*, 2071.
[6] P. T. Anastas, P. Wasserscheid, A. Stark, *Green Solvents: Ionic Liquids*, John Wiley & Sons, **2013**.
[7] N. V. Plechkova, K. R. Seddon, *Chem. Soc. Rev.* **2008**, *37*, 123.
[8] M. Armand, F. Endres, D. R. MacFarlane, H. Ohno, B. Scrosati, *Nat. Mater.* **2009**, *8*, 621.
[9] E. A. Chernikova, L. M. Glukhov, V. G. Krasovskiy, L. M. Kustov, M. G. Vorobyeva, A. A. Koroteev, *Russ. Chem. Rev.* **2015**, *84*, 875.
[10] A. A. Minea, *Int. J. Thermophys.* **2020**, *41*, 1.
[11] E. Fabre, S. S. Murshed, *J. Mater. Chem. A* **2021**.
[12] J. Estager, J. D. Holbrey, M. Swadźba-Kwaśny, *Chem. Soc. Rev.* **2014**, *43*, 847–886.
[13] A. Zazybin, K. Rafikova, V. Yu, D. Zolotareva, V. M. Dembitsky, T. Sasaki, *Russ. Chem. Rev.* **2017**, *86*, 1254.
[14] A. V. Yermalayeu, M. A. Varfolomeev, S. P. Verevkin, *J. Mol. Liq.* **2020**, *317*, 114150.
[15] K. Goossens, K. Lava, C. W. Bielawski, K. Binnemans, *Chem. Rev.* **2016**, *116*, 4643.
[16] S. Tsuzuki, H. Matsumoto, W. Shinoda, M. Mikami, *Phys. Chem. Chem. Phys.* **2011**, *13*, 5987.
[17] H. Weingärtner, *Angew. Chem. Int. Ed.* **2008**, *47*, 654.
[18] F. D. Saeva, *Liquid Crystals: The Fourth State of Matter*, M. Dekker, **1979**.
[19] A. Jákli, *One-and Two-Dimensional Fluids: Properties of Smectic, Lamellar and Columnar Liquid Crystals*, CRC Press, **2006**.

[20] G. W. Gray, V. Vill, H. W. Spiess, D. Demus, J. W. Goodby, *Physical Properties of Liquid Crystals*, John Wiley & Sons, **2009**.
[21] D. Demus, J. W. Goodby, G. W. Gray, H. W. Spiess, V. Vill, *Handbook of Liquid Crystals, Volume 2A: Low Molecular Weight Liquid Crystals I: Calamitic Liquid Crystals*, John Wiley & Sons, **2011**.
[22] J. W. Goodby, P. J. Collings, T. Kato, C. Tschierske, H. Gleeson, P. Raynes, V. Vill, *Handbook of Liquid Crystals, 8 Volume Set*, John Wiley & Sons, **2014**.
[23] J. P. Lagerwall, F. Giesselmann, *ChemPhysChem* **2006**, *7*, 20.
[24] C. Tschierske, *J. Mater. Chem.* **1998**, *8*, 1485.
[25] A. Basile, M. Hilder, F. Makhlooghiazad, C. Pozo-Gonzalo, D. R. MacFarlane, P. C. Howlett, M. Forsyth, *Adv. Energy Mater.* **2018**, *8*, 1703491.
[26] H. Zhu, D. R. MacFarlane, J. M. Pringle, M. Forsyth, *Trends Chem.* **2019**, *1*, 126.
[27] J. Timmermans, *J Chim Phys* **1938**, *35*, 331.
[28] D. R. MacFarlane, P. Meakin, N. Amini, M. Forsyth, *J. Phys. Condens. Matter* **2001**, *13*, 8257.
[29] C. W. Tang, S. A. VanSlyke, *App. Phys. Lett.* **1987**, *51*, 913.
[30] A. Salehi, X. Fu, D. Shin, F. So, *Adv. Funct. Mater.* **2019**, *29*, 1808803.
[31] Q. Pei, G. Yu, C. Zhang, Y. Yang, A. J. Heeger, *Science* **1995**, *269*, 1086.
[32] Li, Z., Meng, H., Li, Z.R., *Organic Light-Emitting Materials and Devices*, CRC Press, Boca Raton, **2006**.
[33] J. Bauri, R. B. Choudhary, G. Mandal, *J. Mater. Sci.* **2021**, *56*, 18837–18866.
[34] S. Tang, L. Edman, in *Photoluminescent Mater. Electroluminescent Devices*, Springer Cham, **2017**, pp. 375–395.
[35] K. Schlingman, Y. Chen, R. S. Carmichael, T. B. Carmichael, *Adv. Mater.* **2021**, 2006863.
[36] Z. Yu, L. Li, H. Gao, Q. Pei, *Sci. China Chem.* **2013**, *56*, 1075.
[37] J. Gao, *Curr. Opin. Electrochem.* **2018**, *7*, 87.
[38] S. Hu, J. Gao, *Adv. Funct. Mater.* **2020**, *30*, 1907003.
[39] S. Hu, H.-W. Yeh, J. Gao, *Mater. Chem. Front.* **2021**, *5*, 1847.
[40] R. D. Costa, E. Ortí, H. J. Bolink, F. Monti, G. Accorsi, N. Armaroli, *Angew. Chem. Int. Ed.* **2012**, *51*, 8178.
[41] D. Ma, T. Tsuboi, Y. Qiu, L. Duan, *Adv. Mater.* **2017**, *29*, 1603253.

[42] M. Martínez-Alonso, J. Cerdá, C. Momblona, A. Pertegás, J. M. Junquera-Hernández, A. Heras, A. M. Rodríguez, G. Espino, H. Bolink, E. Ortí, *Inorg. Chem.* **2017**, *56*, 10298–10310.
[43] S. Karimi, H. Shahroosvand, S. Bellani, F. Bonaccorso, *J. Phys. Chem. C* **2021**, *125*, 819.
[44] L. M. Cavinato, S. Wölfl, A. Pöthig, E. Fresta, C. Garino, J. Fernandez-Cestau, C. Barolo, R. D. Costa, *Adv. Mater.* **2022**, *34*, 2109228.
[45] W. K. Bae, J. Lim, D. Lee, M. Park, H. Lee, J. Kwak, K. Char, C. Lee, S. Lee, *Adv. Mater.* **2014**, *26*, 6387.
[46] H. Jia, Z. Wang, T. Yuan, F. Yuan, X. Li, Y. Li, Z. Tan, L. Fan, S. Yang, *Adv. Sci.* **2019**, *6*, 1900397.
[47] Y.-H. Won, O. Cho, T. Kim, D.-Y. Chung, T. Kim, H. Chung, H. Jang, J. Lee, D. Kim, E. Jang, *Nature* **2019**, *575*, 634.
[48] H. Moon, W. Lee, J. Kim, D. Lee, S. Cha, S. Shin, H. Chae, *Chem. Commun.* **2019**, *55*, 13299.
[49] C.-Y. Han, S.-H. Lee, S.-W. Song, S.-Y. Yoon, J.-H. Jo, D.-Y. Jo, H.-M. Kim, B.-J. Lee, H.-S. Kim, H. Yang, *ACS Energy Lett.* **2020**, *5*, 1568.
[50] S.-Y. Yoon, Y.-H. Kim, D.-Y. Jo, J.-H. Jo, S.-H. Lee, H.-M. Kim, Y. Kim, S.-K. Kim, H. Yang, *Chem. Eng. J.* **2021**, *410*, 128426.
[51] E. Fresta, R. D. Costa, *J. Mater. Chem. C* **2017**, *5*, 5643.
[52] J. Choi, S. Kanagaraj, Y. Choe, *J. Mater. Chem. C* **2020**, *8*, 4580–4587.
[53] T. Zhang, R. Xu, H. Lv, Z. Wang, H. Ye, H. Liu, L. Chen, *Optik* **2022**, *261*, 169176.
[54] H.-L. Shen, P.-W. Hsiao, R.-H. Yi, Y.-H. Su, Y. Chen, C.-W. Lu, H.-C. Su, *Dyes Pigments* **2022**, *203*, 110346.
[55] A. Puthanveedu, K. Shanmugasundaram, S. Yoon, Y. Choe, *J Mater Chem C* **2022**, *10*, 2245–2254.
[56] J. -K. Lee, D. S. Yoo, E. S. Handy, M. F. Rubner, *Appl. Phys. Lett.* **1996**, *69*, 1686.
[57] M. A. Baldo, D. F. O'Brien, Y. You, A. Shoustikov, S. Sibley, M. E. Thompson, S. R. Forrest, *Nature* **1998**, *395*, 151.
[58] P. D. Fleischauer, Patricia. Fleischauer, *Chem. Rev.* **1970**, *70*, 199.
[59] A. J. Lees, *Chem. Rev.* **1987**, *87*, 711.
[60] J. H. Burroughes, D. D. C. Bradley, A. R. Brown, R. N. Marks, K. Mackay, R. H. Friend, P. L. Burns, A. B. Holmes, *Nature* **1990**, *347*, 539.
[61] A. R. Brown, K. Pichler, N. C. Greenham, D. D. C. Bradley, R. H. Friend, A. B. Holmes, *Chem. Phys. Lett.* **1993**, *210*, 61.

[62] M. A. Baldo, D. F. O'Brien, M. E. Thompson, S. R. Forrest, *Phys Rev B* **1999**, *60*, 14422.
[63] M. A. Baldo, M. E. Thompson, S. R. Forrest, *Pure Appl. Chem.* **1999**, *71*, 2095.
[64] H. Shin, Y. H. Ha, H.-G. Kim, R. Kim, S.-K. Kwon, Y.-H. Kim, J.-J. Kim, *Adv. Mater.* **2019**, *31*, 1808102.
[65] Q. Li, C. Shi, M. Huang, X. Wei, H. Yan, C. Yang, A. Yuan, *Chem. Sci.* **2019**, *10*, 3257.
[66] C. Zhang, R. Liu, D. Zhang, L. Duan, *Adv. Funct. Mater.* **2020**, *30*, 1907156.
[67] G. Hong, X. Gan, C. Leonhardt, Z. Zhang, J. Seibert, J. M. Busch, S. Bräse, *Adv. Mater.* **2021**, *33*, 2005630.
[68] R. Bai, X. Meng, X. Wang, L. He, *Adv. Funct. Mater.* **2020**, *30*, 1907169.
[69] S. Kanagaraj, A. Puthanveedu, Y. Choe, *Adv. Funct. Mater.* **2020**, *30*, 1907126.
[70] J. E. Namanga, H. Pei, G. Bousrez, V. Smetana, N. Gerlitzki, A.-V. Mudring, *ACS Appl. Energy Mater.* **2020**, *3*, 9271.
[71] J. E. Namanga, H. Pei, G. Bousrez, B. Mallick, V. Smetana, N. Gerlitzki, A.-V. Mudring, *Adv. Funct. Mater.* **2020**, *30*, 1909809.
[72] R. Hamze, J. L. Peltier, D. Sylvinson, M. Jung, J. Cardenas, R. Haiges, M. Soleilhavoup, R. Jazzar, P. I. Djurovich, G. Bertrand, M. E. Thompson, *Science* **2019**, *363*, 601.
[73] P. Tao, S. Liu, W. Wong, *Adv. Opt. Mater.* **2020**, *8*, 2000985.
[74] G. Hu, B. Xu, A. Wang, Y. Guo, J. Wu, F. Muhammad, W. Meng, C. Wang, S. Sui, Y. Liu, Y. Li, Y. Zhang, Y. Zhou, Z. Deng, *Adv. Funct. Mater.* **2021**, *31*, 2011191.
[75] H.-C. Su, Y.-R. Chen, K.-T. Wong, *Adv. Funct. Mater.* **2020**, *30*, 1906898.
[76] C. W. Tang, S. A. VanSlyke, C. H. Chen, *J. Appl. Phys.* **1989**, *65*, 3610.
[77] W. Ning, F. Gao, *Adv. Mater.* **2019**, *31*, 1900326.
[78] Z. Xiao, Z. Song, Y. Yan, *Adv. Mater.* **2019**, *31*, 1803792.
[79] M. Li, Z. Xia, *Chem. Soc. Rev.* **2021**, *50*, 2626.
[80] U. Lanver, G. Lehmann, *J. Lumin.* **1978**, *17*, 225–235.
[81] A. S. Berezin, K. A. Vinogradova, V. A. Nadolinny, T. S. Sukhikh, V. P. Krivopalov, E. B. Nikolaenkova, M. B. Bushuev, *Dalton Trans* **2018**, *47*, 1657.
[82] V. Morad, I. Cherniukh, L. Pöttschacher, Y. Shynkarenko, S. Yakunin, M. V. Kovalenko, *Chem. Mater.* **2019**, *31*, 10161–10169.

[83] L.-K. Gong, Q.-Q. Hu, F.-Q. Huang, Z.-Z. Zhang, N.-N. Shen, B. Hu, Y. Song, Z.-P. Wang, K.-Z. Du, X.-Y. Huang, *Chem. Commun.* **2019**, *55*, 7303.
[84] B. Su, M. S. Molokeev, Z. Xia, *J. Mater. Chem. C* **2019**, *7*, 11220.
[85] M. Bortoluzzi, J. Castro, A. Gobbo, V. Ferraro, L. Pietrobon, S. Antoniutti, *New J Chem* **2020**, *44*, 571.
[86] M. Bortoluzzi, V. Ferraro, J. Castro, *Dalton Trans* **2021**, *50*, 3132.
[87] C. Jiang, L. Qianqian, C. Luo, H. Lin, H. Peng, *J. Phys. Condens. Matter* **2022**.
[88] Z. Huang, M. Yi, Y. Xu, P. Qi, Y. Liu, A. Song, J. Hao, *J. Mater. Chem. C* **2021**, *9*, 13276.
[89] L.-J. Xu, C.-Z. Sun, H. Xiao, Y. Wu, Z.-N. Chen, *Adv. Mater.* **2017**, *29*, 1605739.
[90] M. Worku, Y. Tian, C. Zhou, S. Lee, Q. Meisner, Y. Zhou, B. Ma, *ACS Appl. Mater. Interfaces* **2018**, *10*, 30051.
[91] L. Mao, P. Guo, S. Wang, A. K. Cheetham, R. Seshadri, *J. Am. Chem. Soc.* **2020**, *142*, 13582–13589.
[92] E. Fresta, R. D. Costa, *J. Mater. Chem. C* **2017**, *5*, 5643.
[93] M. S. Subeesh, K. Shanmugasundaram, C. D. Sunesh, T. P. Nguyen, Y. Choe, *J. Phys. Chem. C* **2015**, *119*, 23676.
[94] M. Y. Wong, M.-G. La-Placa, A. Pertegas, H. J. Bolink, E. Zysman-Colman, *J. Mater. Chem. C* **2017**, *5*, 1699.
[95] A. M. Bünzli, E. C. Constable, C. E. Housecroft, A. Prescimone, J. A. Zampese, G. Longo, L. Gil-Escrig, A. Pertegás, E. Ortí, H. J. Bolink, *Chem. Sci.* **2015**, *6*, 2843.
[96] J. Mindemark, S. Tang, J. Wang, N. Kaihovirta, D. Brandell, L. Edman, *Chem. Mater.* **2016**, *28*, 2618.
[97] H.-F. Chen, C.-T. Liao, T.-C. Chen, H.-C. Su, K.-T. Wong, T.-F. Guo, *J. Mater. Chem.* **2011**, *21*, 4175.
[98] M. S. Subeesh, K. Shanmugasundaram, C. D. Sunesh, Y. S. Won, Y. Choe, *J. Mater. Chem. C* **2015**, *3*, 4683.
[99] J. Kido, Y. Iizumi, *Chem. Lett.* **1997**, *26*, 963.
[100] S. So, K. Lee, W. Choi, L. Leung, W. Lo, *Jpn. J. Appl. Phys.* **2001**, *40*, 5959.
[101] M. Cölle, R. E. Dinnebier, W. Brütting, *Chem Commun* **2002**, 2908.
[102] P. Kumar, A. Misra, R. Bhardwaj, M. N. Kamalasanan, S. C. Jain, S. Chand, R. P. Tandon, *Displays* **2008**, *29*, 351.
[103] C. W. Tang, S. A. VanSlyke, *Appl. Phys. Lett.* **1987**, *51*, 913.
[104] S.-Y. Park, P. Ghosh, S. O. Park, Y. M. Lee, S. K. Kwak, O.-H. Kwon, *RSC Adv.* **2016**, *6*, 9812.

[105] S. Schulman, Q. Fernando, *Tetrahedron* **1968**, *24*, 1777.
[106] S. G. Schulman, *Anal. Chem.* **1971**, *43*, 285.
[107] R. E. Ballard, J. W. Edwards, *J. Chem. Soc. Resumed* **1964**, 4868.
[108] J. Barber, *Chem. Soc. Rev.* **2009**, *38*, 185.
[109] H. M. D. Bandara, S. C. Burdette, *Chem. Soc. Rev.* **2012**, *41*, 1809.
[110] A. Cembran, F. Bernardi, M. Garavelli, L. Gagliardi, G. Orlandi, *J. Am. Chem. Soc.* **2004**, *126*, 3234.
[111] J. Dokić, M. Gothe, J. Wirth, M. V. Peters, J. Schwarz, S. Hecht, P. Saalfrank, *J. Phys. Chem. A* **2009**, *113*, 6763.
[112] A. Natansohn, P. Rochon, J. Gosselin, S. Xie, *Macromolecules* **1992**, *25*, 2268.
[113] T. Ikeda, O. Tsutsumi, *Science* **1995**, *268*, 1873.
[114] S. Shinkai, T. Nakaji, T. Ogawa, K. Shigematsu, O. Manabe, *J. Am. Chem. Soc.* **1981**, *103*, 111.
[115] IEA, "Global Energy Review 2020: The impacts of the Covid-19 crisis on global energy demand and CO2 emissions", can be found under https://www.iea.org/reports/global-energy-review-2020, **2020**.
[116] P. Jiang, Y. V. Fan, J. J. Klemeš, *Appl. Energy* **2021**, *285*, 116441.
[117] IEA, "The Covid-19 crisis is causing the biggest fall in global energy investment in history", can be found under https://www.iea.org/news/the-covid-19-crisis-is-causing-the-biggest-fall-in-global-energy-investment-in-history, **2020**.
[118] Lewis, N. S., "Basic Research Needs for Solar Energy Utilization" can be found under https://www.osti.gov/servlets/purl/899136-uy8Fy6/, **2005**.
[119] W. Shockley, H. J. Queisser, *J. Appl. Phys.* **1961**, *32*, 510.
[120] G. Boschloo, A. Hagfeldt, *Acc. Chem. Res.* **2009**, *42*, 1819.
[121] M. Grätzel, *Nature* **2001**, *414*, 338.
[122] S. M. Zakeeruddin, M. Grätzel, *Adv. Funct. Mater.* **2009**, *19*, 2187.
[123] T.-Y. Cho, S.-G. Yoon, S. S. Sekhon, C.-H. Han, *Bull. Korean Chem. Soc.* **2011**, *32*, 2058–2062.
[124] G. P. S. Lau, J.-D. Décoppet, T. Moehl, S. M. Zakeeruddin, M. Grätzel, P. J. Dyson, *Sci. Rep.* **2015**, *5*, 18158.
[125] A. Lennert, M. Sternberg, K. Meyer, R. D. Costa, D. M. Guldi, *ACS Appl. Mater. Interfaces* **2017**, *9*, 33437.

[126] S. Denizalti, A. K. Ali, Ç. Ela, M. Ekmekci, S. Erten-Ela, *Chem. Phys. Lett.* **2018**, *691*, 373.
[127] B. O'Regan, M. Grätzel, *Nature* **1991**, *353*, 737.
[128] H. Matsumoto, T. Matsuda, *Electrochemistry* **2002**, *70*, 190.
[129] N. Yamanaka, R. Kawano, W. Kubo, T. Kitamura, Y. Wada, M. Watanabe, S. Yanagida, *Chem. Commun.* **2005**, 740–742.
[130] N. Yamanaka, R. Kawano, W. Kubo, N. Masaki, T. Kitamura, Y. Wada, M. Watanabe, S. Yanagida, *J Phys Chem B* **2007**, *111*, 4763.
[131] M. Gorlov, L. Kloo, *Dalton Trans.* **2008**, 2655–2666.
[132] Y. Qin, P. She, X. Huang, W. Huang, Q. Zhao, *Coord. Chem. Rev.* **2020**, *416*, 213331.
[133] M. Wrighton, D. Ginley, *Chem. Phys.* **1974**, *4*, 295.
[134] R. Bai, X. Meng, X. Wang, L. He, *Adv. Funct. Mater.* **2021**, *31*, 2007167.
[135] S. Tang, P. Murto, J. Wang, C. Larsen, M. R. Andersson, E. Wang, L. Edman, *Adv. Opt. Mater.* **2019**, *7*, 1900451.
[136] S. Tang, H. A. Buchholz, L. Edman, *J. Mater. Chem. C* **2015**, *3*, 8114.
[137] A. Pertegás, N. M. Shavaleev, D. Tordera, E. Ortí, M. K. Nazeeruddin, H. J. Bolink, *J. Mater. Chem. C* **2014**, *2*, 1605.
[138] Y. Rodríguez-Lazcano, L. Nataf, F. Rodríguez, *Phys. Rev. B* **2009**, *80*, 085115.
[139] P. Bonhôte, A.-P. Dias, N. Papageorgiou, K. Kalyanasundaram, M. Grätzel, *Inorg. Chem.* **1996**, *35*, 1168.
[140] J. Sun, M. Forsyth, D. R. MacFarlane, *J. Phys. Chem. B* **1998**, *102*, 8858.
[141] J. S. Yadav, B. V. S. Reddy, Ch. S. Reddy, K. Rajasekhar, *J. Org. Chem.* **2003**, *68*, 2525.
[142] S. F. Lux, L. Terborg, O. Hachmöller, T. Placke, H.-W. Meyer, S. Passerini, M. Winter, S. Nowak, *J. Electrochem. Soc.* **2013**, *160*, A1694.
[143] D. Painuly, R. Singhal, P. Kandwal, I. M. Nagpure, *J. Electron. Mater.* **2020**, *49*, 6096.
[144] S. Wu, X. Zhong, H. Zeng, W. You, W. Zhou, *J. Lumin.* **2018**, *195*, 120.
[145] J. Tan, X. Li, Y. Zhan, J. Xiong, X. Lv, C. Pan, Y. Huo, *Polyhedron* **2018**, *155*, 398.
[146] Y. Y. Wang, Y. Ren, J. Liu, C. Q. Zhang, S. Q. Xia, X. T. Tao, *Dyes Pigments* **2016**, *133*, 9.

[147] C. Pérez-Bolívar, S. Takizawa, G. Nishimura, V. A. Montes, P. Anzenbacher Jr, *Chem. Eur. J.* **2011**, *17*, 9076.
[148] H. Wang, B. Xu, X. Liu, H. Zhou, Y. Hao, H. Xu, L. Chen, *Org. Electron.* **2009**, *10*, 918.
[149] M. Saccone, F. F. Palacio, G. Cavallo, V. Dichiarante, M. Virkki, G. Terraneo, A. Priimagi, P. Metrangolo, *Faraday Discuss* **2017**, *203*, 407.
[150] A. Abbaszad Rafi, N. Hamidi, A. Bashir-Hashemi, M. Mahkam, *ACS Biomater. Sci. Eng.* **2018**, *4*, 184.
[151] S. Xiao, X. Lu, Q. Lu, B. Su, *Macromolecules* **2008**, *41*, 3884.
[152] Q. Zhang, C. Shan, X. Wang, L. Chen, L. Niu, B. Chen, *Liq. Cryst.* **2008**, *35*, 1299.
[153] V. W.-W. Yam, J. K.-W. Lee, C.-C. Ko, N. Zhu, *J. Am. Chem. Soc.* **2009**, *131*, 912.
[154] S. Zhang, S. Liu, Q. Zhang, Y. Deng, *Chem Commun* **2011**, *47*, 6641.
[155] K. Stappert, J. Muthmann, E. T. Spielberg, A.-V. Mudring, *Cryst. Growth Des.* **2015**, *15*, 4701.
[156] P. P. Birnbaum, J. H. Linford, D. W. G. Style, *Trans Faraday Soc* **1953**, *49*, 735.
[157] R. D. Costa, F. Werner, X. Wang, P. Grönninger, S. Feihl, F. T. U. Kohler, P. Wasserscheid, S. Hibler, R. Beranek, K. Meyer, D. M. Guldi, *Adv. Energy Mater.* **2013**, *3*, 657.
[158] D. Högberg, B. Soberats, R. Yatagai, S. Uchida, M. Yoshio, L. Kloo, H. Segawa, T. Kato, *Chem. Mater.* **2016**, *28*, 6493.
[159] K. Stappert, D. Ünal, B. Mallick, A.-V. Mudring, *J. Mater. Chem. C* **2014**, *2*, 7976.
[160] K. Stappert, D. Unal, E. T. Spielberg, A.-V. Mudring, *Cryst. Growth Des.* **2015**, *15*, 752.
[161] K. Stappert, A.-V. Mudring, *RSC Adv.* **2015**, *5*, 16886.